CATÓLICA
ESCOLA SUPERIOR DE BIOTECNOLOGIA
PORTO

Exploiting anticancer and antimicrobial activities of biosynthetic gold nanoparticles by *Pseudomonas aeruginosa* (PAO1)

By Marco Neves Castanheira Melo Oliveira

December 2022

CATÓLICA
ESCOLA SUPERIOR DE BIOTECNOLOGIA
PORTO

Exploiting anticancer and antimicrobial activities of biosynthetic gold nanoparticles by *Pseudomonas aeruginosa* (PAO1)

Thesis presented to *Escola Superior de Biotecnologia of the Universidade Católica Portuguesa* to fulfil the requirements of Master of Science degree in Applied Microbiology

---

By Marco Neves Castanheira Melo Oliveira

Supervisor: Professor Ruben Fernandes

Co-supervisor: Doctor Carla Pereira

December 2022

Abstract

Biosynthetic gold nanoparticles (bAuNPs) have emerged as a disruptive, eco-friendly and cost-effective alternative to overcome the limitations of conventional synthesis methods, namely, the need to use hazardous chemicals and high temperatures. Among the wide range of possible applications of bAuNPs, their potential as atitumor and antimicrobial agents has been explored. However, there are limited studies that describe the dependence on physicochemical parameters to control the shape, size, aggregation, and yields during bAuNP synthesis. Some studies have used *Pseudomonas aeruginosa* (PAO1) extracts for the biological synthesis of AuNPs. The main focus of the present study was to disclose which conditions of PAO1 cultures lead to higher bAuNPs synthesis yields, to understand the influence of different conditions on bAuNPs biosynthesis (temperature, pH and incubation period), and to evaluate how bAuNPs shapes and sizes affect the antibacterial and antitumor activity. UV-Vis spectroscopy, TEM, and ATR-FT-IR analysis were used to characterize the biosynthetic AuNPs. It is speculated that bAuNPs are produced by means of redox reactions. In this sense, DCIP (2,6-Dichlorophenolindophenol) was used as an indicator of the reduction potential of PAO1. It was exploited both anticancer and antibacterial to disclose the bAuNPs biological activity. An anticancer screening of bAuNP activity was performed on prostate cell carcinoma. A model concerning normal and neoplastic epithelial cells were used in the present study. *In vitro* assays were performed using the neoplastic prostate cell line PC3 and the normal epithelial cell (HPEpiC). Cellular viability, cellular proliferation, cellular migration, and Interleukin 6 (IL-6) levels were determined. The activity of bAuNPs on bacteria was screened in bacteria growth (kinetics) and in viability, in two Gram-negative bacteria and in one Gram-positive bacterium. PC3 cancer cells were most affected by bAuNPs synthesized at pH 9.0 for 24h and at 58 ºC showing a significant reduction in cell viability, cellular migration, and IL-6 levels of PC3 cells without significant effects in HPEpiC cells. Regarding the antimicrobial assays, the effect on bacterial growth and viability was more significant in Gram-negative bacteria. Furthermore, bAuNPs synthesis at pH 9.0 for 24 h at 58ºC prompted smaller, more spherical, and less aggregated bAuNPs. These properties may enhance the internalization of bAuNPs in cells, thereby increasing both antitumor and antibacterial activity. Along with the bioactive potential of bAuNPs, the control of shape, size, and aggregation could be used to improve therapeutic approaches for prostate cancer and bacterial infections, contributing for more targeted, cheaper, and greener therapies.

Keywords: *Pseudomonas aeruginosa*, biosynthetic gold nanoparticles, prostate cancer, bacteria.

Resumo

As nanopartículas de ouro biossintéticas (bAuNPs) têm surgido como uma alternativa disruptiva, ecológica e rentável para os métodos de síntese convencionais, reduzindo a necessidade de utilizar compostos químicos perigosos e temperaturas elevadas. De entre a vasta gama de possíveis aplicações das bAuNPs, o seu potencial como agentes antitumorais e antimicrobianos tem vindo a ser explorado. Contudo, existem estudos limitados que descrevem a dependência dos parâmetros físico-químicos para controlar a forma, tamanho, agregação, e rendimentos durante a síntese de bAuNPs. Alguns estudos têm utilizado extratos de *Pseudomonas aeruginosa* (PAO1) para a síntese biológica de AuNPs. O foco principal do presente estudo foi revelar quais as condições de cultura de PAO1 que permitem obter maiores rendimentos de síntese de bAuNPs, compreender a influencia de diferentes condições da biossíntese das bAuNPs (temperatura, pH e período de incubação), e avaliar como as formas e tamanhos das bAuNPs afetam a sua atividade antitumoral e antibacteriana. A caracterização das bAuNPs foi realizada por meio de espectroscopia UV-Vis, TEM e ATR-FT-IR. Especula-se que as bAuNPs sejam produzidas por reações de oxirredução. Neste sentido, o DCIP (2,6-Diclorofenolindofenol) foi utilizado como indicador do potencial de redução da PAO1. Foi explorado tanto o potencial antitumoral como antibacteriano de forma a revelar a atividade biológica das bAuNPs. A atividade antitumoral foi avaliada através de ensaios *in vitro* utilizando a linha de células neoplásicas da próstata PC3 e de células epiteliais normais da próstata (HPEpiC). Foi avaliada a viabilidade celular, proliferação celular, migração celular e os níveis de Interleucina 6 (IL-6). O potencial antimicrobiano das bAuNPs foi avaliado tanto no crescimento (cinética) como na viabilidade bacteriana, em duas bactérias Gram-negativas e numa bactéria Gram-positiva. As bAuNPs sintetizadas a pH 9.0 durante 24 h e a 58 ºC induziram uma redução significativa na viabilidade celular, migração celular, e níveis IL-6 nas células PC3 sem revelar efeitos significativos nas células HPEpiC. Em relação aos ensaios antimicrobianos, o efeito no crescimento e viabilidade bacteriana foi mais significativo nas bactérias Gram-negativas. Além disso, a síntese de bAuNPs a pH 9.0 durante 24 h a 58 ºC permitiu a obter bAuNPs mais pequenas, mais esféricas, e menos agregadas. Estas propriedades podem assim melhorar a internalização de bAuNPs nas células, permitindo aumentar tanto a atividade antitumoral como antibacteriana. Desta forma, juntamente com o potencial bioativo das bAuNPs, o controlo da forma, tamanho e agregação poderia contribuir para o desenvolvimento de terapias mais direcionadas, mais baratas, e mais ecológicas.

Palavras-chave: *Pseudomonas aeruginosa*, nanopartículas de ouro biossintéticas, cancro da próstata, bactérias.

Dedicatória

Esta tese é dedicada a um grande homem, ex-combatente da guerra colonial portuguesa, ao meu avô, Álvaro Pacheco De Melo. Este, apesar de todas as peripécias e aventuras que gostava de recordar de forma inspiradora a quem o rodeasse, acabou por abandonar esta vida a lutar até ao fim contra um adversário, desta vez mais exigente, o cancro da próstata.

Agradecimentos

Gostaria de prestar os meus maiores e mais sinceros agradecimentos a todas as pessoas que contribuíram para este trabalho, o qual foi capaz de prevenir muitas horas de sono. Primeiramente, agradecer aos meus pais, à minha irmã, aos meus avós e toda a família. Pessoas incansáveis e a fundação de toda a minha motivação e estabilidade emocional. Deixar um agradecimento com muito carinho ao Professor Ruben Fernandes e à Doutora Pilar Baylina por me permitirem ficar no laboratório até altas horas da manhã, pelos debates científicos profundos, pelas dores de cabeça que possa ter causado, por toda a inspiração e motivação e por serem os meus dois baluartes no mundo das ciências. O meu obrigado à Doutora Carla Pereira e ao Doutor António Cesar pela disponibilidade e trabalho prestados. Agradecer a incansável ajuda da Silvia Soares, a qual desde o primeiro dia encarou este trabalho como sendo próprio e procurou todos os seus meios para fazer com que este atingisse o seu maior potencial. Por extensão, surge o meu agradecimento ao Doutor Miguel Correa (Universidade de Vigo) por toda a ajuda prestada na caraterização das nanopartículas.

Gostaria também de agradecer a todos os meu colegas de mestrado e colaboradores do LaBMI. Aqueles que me ajudaram a conciliar o mestrado com todo o trabalho no laboratório que paralelemente me encontrava a desenvolver. Entre longas noites a aprofundar o trabalho da minha tese e outras quantas a tratar amostras da Covid-19 tentando dar resposta aos desafios que a pandemia trouxe para o país e para o mundo. Assim, torna-se para mim fundamental referir os nomes da minha equipa e daqueles que estiveram comigo desde o início: André Sousa, Catarina Teixeira, Sara, Raquel, Catarina Rocha, Carla Guedes, Marlene, Sofia, Vitorino, Maria, Diogo Cabral, Frantz, João, Gonçalo, Diogo Ferreira, Cátia, Carla Luís, Claúdia e Fábio. Posso desta forma dizer que sou uma pessoa de sorte, pois tenho uma segunda família repleta de pessoas excecionais e extremamente profissionais.

Por último, e por falar em segunda família, não posso deixar esta sessão de agradecimentos sem um obrigado especial a todos os meus amigos. Ao Tiago, ao Luís, ao Manuel, ao Rodrigo, à Natacha, à Maria, ao César, ao António, à Bruna, às Danielas, à Rita e a todos os elementos da Tuna TS. Por todas as conversas casuais de quais muitas ideias surgiram, pelas boleias para o trabalho e para a universidade, pelos cafés, por me erguerem o estado de espírito, por fazerem de mim aquilo que sou hoje.

Mais uma vez, um muito obrigado a todos!

Table of Contents

Abstract 5

Resumo 7

Dedicatória 9

Agradecimentos 10

Abbreviations list 14

1. Introduction 17

1.1 Gold nanoparticles 17

1.2 *Pseudomonas aeruginosa* 21

1.4 Prostate cancer and gold nanoparticles 22

1.5 Bacteria and gold nanoparticles 24

1.5.1 Gram-negative bacteria 25

1.5.2 Gram-positive bacteria 25

1.7 Work relevance 27

2. Methodology 28

2.1 AuNP biosynthesis - Optimization and Characterization 28

2.1.1 *Pseudomonas aeruginosa* strain and maintenance 28

2.1.2 Optimization of the bacterial growth conditions for maximum reduction potential 28

2.1.3 Confirmation of DCIP method as an indicator of PAO1 reduction potential and investigation of GR gene possible involvement in AuNPs biosynthesis 29

2.1.4 Biosynthesis of AuNP at different physicochemical conditions 30

2.1.4.1 Characterization of biosynthesized bAuNPs 31

2.2 bAuNP against prostate cancer 32

2.2.1 Cytotoxic effect evaluation of the bAuNPs in prostate cell lines 32

2.2.1.1 Cell culture and treatments 32

2.3 AuNPs against Gram-positive and Gram-negative bacteria 35

2.3.1 AuNPs effect on bacteria growth – Kinetics 35
2.3.2 AuNPs effect on the viability of *E. coli* and MRSA 36
3. Results 37
3.1 Optimization of the bacterial growth conditions for maximum reduction potential 37
3.1.1 DCIP Method 37
3.1.2 Confirmation of DCIP method as an indicator of PAO1 reduction potential and investigation of GR gene possible involvement in AuNPs biosynthesis 38
3.1.3 Biosynthesis and characterization of AuNPs 39
3.2 Cytotoxic effect evaluation of bAuNPs in prostate cell lines 46
3.2.1 bAuNPs cellular uptake assay 46
3.2.2 Viability and Proliferation assay 46
3.2.3 Injury 47
3.2.4 Human interleukin 6 (IL-6) ELISA assay 48
3.3 AuNPs against Gram-positive and Gram-negative bacteria 49
3.3.1 AuNPs effect on bacteria growth – Kinetics 49
3.3.2 AuNPs effect on the viability of *E. coli* and MRSA 51
4. Discussion 53
5. Conclusion 58
6. Future Perspectives 59
7. Bibliography 60
8. Appendix 68
8.1 Appendix 1 68
8.2 Appendix 2 69
8.3 Appendix 3 70
8.4 Appendix 4 71
8.5 Appendix 5 72

Abbreviations list

AgNPs – Silver nanoparticles

Anti-BrdU-POD - Antibody-bromodeoxyuridine-peroxidase

ATCC - American Type Culture Collection

ATP - Adenosine triphosphate

ATPase - Adenosine triphosphatase

ATR-FT-IR – Attenuated Total reflection Fourier – Transform Infrared Spectroscopy

AuNPs – Gold nanoparticles

bAuNPs – Biosynthesized gold nanoparticles

BPH - Benign prostatic hyperplasia

BrdU - Bromodeoxyuridine

CFU – Colony Forming Units

Cur-AuNPs – Curcumin coated gold nanoparticles

DAPI - 4′,6-diamidino-2-phenylindole

DCIP - 2,6-Dichlorophenolindophenol

DNA - Deoxyribonucleic Acid

ELISA - Enzyme-linked immunosorbent assay

GR – Glutathione – reductase – encoding gene

GSH – Glutathione

GSSG – Glutathione disulfide

ICP-MS - Inductively coupled plasma mass spectroscopy

ID - Identity

IL-6 – Interleukin 6

IMARC - International Market Analysis Research and Consulting Group

LaBMI – Laboratory of Medical and Industrial Biotechnology

MHA – Muller-Hinton Agar

MHB – Muller-Hinton Broth

MRSA – Methicillin - Resistant *Staphylococcus aureus*

MSSA - Methicillin-susceptible *Staphylococcus aureus*

MTT - 3-[4,5-dimethylthiazol-2-yl]-2,5 diphenyl tetrazolium bromide

NADP – Reduced form of nicotinamide-adenine dinucleotide phosphate

NADPH – Nicotinamide-adenine dinucleotide phosphate

NPs – Nanoparticles

OD – Optical Density

PAO1 – *Pseudomonas aeruginosa* strain PAO1

PBS - Phosphate buffered saline

PC3 – Human prostate cancer cell lines

PCa – Prostate cancer

PORTIC – Porto Research, Technology & Innovation Center

RhoD - rhodamine B

ROS – Reactive Oxygen Species

RPM – Rotations per Minute

SCCmec - Staphylococcal cassette chromosome mec

SD – Standard Deviation

SPR – Surface Plasmon Resonance

TEM – Transmission Electron Microscopy

tRNA – Transfer ribonucleic acid

TSA – Tryptic Soy Agar

TSB – Tryptic Soy Broth

UTI – Urinary Tract Infections

UV-Vis – Ultraviolet–visible spectroscopy

1. Introduction

Numerous nanomaterials and nanoparticles synthesized by biological, physical, chemical, or even by hybrid methods, have emerged from different building materials such as gold, silver, zinc, iron, silica, copper, and cobalt (1, 2). The tuning of nanoparticles (NPs)' chemical, physical, and biological properties renders a huge versatility for application in different fields, namely as image contrast agents, as vectors for the delivery of drugs or small molecules, and for diagnostic purposes (3). The gold nanoparticles (AuNPs) have gained importance over the years, namely in the biological and pharmaceutical fields, due to their unique optical and physical characteristics that are interesting for their application in different fields (4).

The next subsection (1.1 Gold nanoparticles) discusses the AuNPs' commercial and economic importance, basic characteristics, and key methods of production.

1.1 Gold nanoparticles

In 2021 gold nanoparticles market reached a value of US$ 4.4 Billion globally. Accordingly with IMARC group it is expected to grow US$ 4.5 Billion by 2027 (5). The application of gold nanoparticles to the target drug delivery system has culminated in numerous benefits such as high targeting efficiency, high therapeutic efficacy, and reproducibility. In this way, the drug delivery segment is one of the substantial foundations for the application of gold nanoparticles (6). The market is also benefiting from the efforts focused on modulating the shape and size of gold nanoparticles for upgrading their catalytic, optical and electronic characteristics, which is resulting in novel application areas (7).

The main feature of AuNPs on which its optical potential depends is the Surface Plasmon Resonance (SPR), a resonance phenomenon of gold electrons, which disperse and absorb light in response to incident radiation (Fig. 1.1). In a metallic nanostructure, SPR is described by oscillating electrons obtaining a frequency oscillation equal to the irradiating electromagnetic field (8).

AuNPs optical properties are highly dependent on their size, shape, and structure. The position and width of the plasmon resonance peak can give information about the average diameter and distribution of particle size (9-11). In addition, AuNPs have exhibit tunable properties that lead to particles with various sizes and shapes (nanorodes, nanostars, nanocubes,

nanocages, nanospheres, among others) exhibiting different yields and dispersity, that are dependent on the synthesis parameters (12).

Significant red-shifting of SPR frequency is observed as a consequence of the aggregation between the AuNPs, changing the solution color from red to blue and widening the surface plasmon band (13). The same effect in SPR longitudinal band, and in the color of the colloidal solution, is observed when size changes (14).

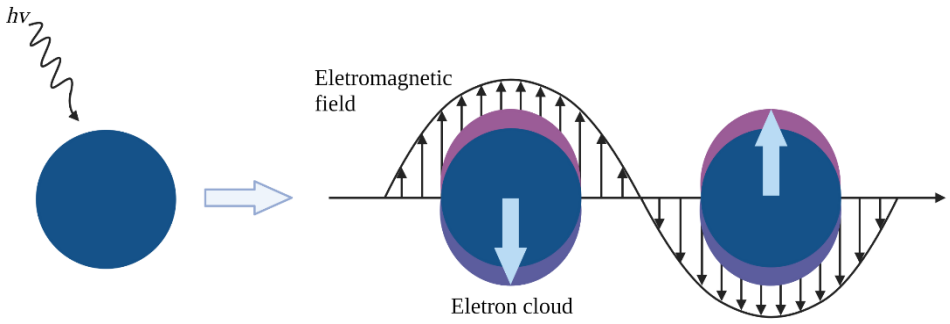

Figure 1.1 - Illustration of the resonance effect of gold electrons in response of incident radiation (8);

Various synthesis methods can be applied to produce AuNPs (Table 1.1). AuNPs are typically synthesized using a chemical reduction process, where gold ions are reduced to their elemental form using a reducing agent. Regarding the conventional chemical methods, the Turkevitch method has been reported as the most widely used, which involves using water containing citrate to reduce $AuCl_4^-$ (12), due to the ease of synthesis, good stability, and controllable size. Radiation (i.e., microwave, gamma irradiation or ultraviolet) is used as typical physical method in AuNPs preparation by creating heat and a reducing environment. Besides radiation-related methods, lasers emitting wavelengths can also be used to produce AuNPs with tunable features, in a commonly used physical method called laser ablation (15).

Table 1.1 - Methods for the AuNPs synthesis and respective reducing agents.

Reference	Synthesis method	Gold ions source	Reducing agent
Singh et al. (16)	Turkevitch	$HAuCl_4$	Citrate;
Weifeng et al. (17)	One-pot	$HAuCl_4$	4-(2-Hydroxyethyl)-1-piperazinyl]-ethanesulfonic acid (HEPES);
Jenkins et al. (18)	Seed-mediated	$HAuCl_4$	Citrate;
Singh et al. (16)	Radiation	$HAuCl_4$	Microwave, gamma irradiation or ultraviolet;
Levy et al. (19)	Laser ablation	Pure gold plate	Not applied (the direct incidence of the laser in a pure gold plate produces AuNPs);
Singh et al. (16)	Biosynthesis	$HAuCl_4$	Microalgae, fungi, bacteria, and plants extracts;

Each synthesis methodology follows two steps of AuNP synthesis: (I) nucleation and (II) growth phase. Nucleation is the process by which in a single-phase system a particle from a new phase, a cluster, is formed. In the chemistry of AuNPs synthesis, these clusters are referred to as nuclei. The critical radius of these clusters is related to the smallest size at which a particle may remain in solution without becoming redissolved. During the growth stage, more material is deposited on the cluster, increasing its size, and transforming it into a nanoparticle. This is governed by the spread of growing species as well as surface processes (20).

Although chemical and other conventional synthesis methods for gold nanocrystals have grown in popularity over the years, the use of hazardous chemicals, high pressures, and temperatures has led to their establishment as less eco-friendly than biosynthetic methods. Thus, biosynthesized nanoparticles have emerged as a disruptive alternative to fill the gaps in conventional synthesis methods. In addition to promote greater sustainability, biosynthesized nanoparticles, due to their avant-garde properties, in terms of biocompatibility, bioavailability,

bioactivity and bioabsorption, have been explored to replace NPs synthetized by conventional synthesis methods in a wide range of applications (21).

Different organisms have been used to produce bAuNPs (*e.g.*, plant tissues, actinomycetes, fungi, bacteria, algae, among others). Some studies have described the intracellular synthesis of bAuNPs for example using fungi. However, this approach becomes more complex and time-consuming when compared with the extracellular synthesis that prompt the elimination of several steps demanded for the recovery of AuNPs (22).

Bacteria have become the broadly studied microorganism and are preferred for the synthesis of NPs due to its undemanding conditions, ease of purification and good synthesis yields. A variety of bacterial strains has been used to produce bAuNPs, among them it is possible to find in the literature *P. aeruginosa, E. coli* DH5α*, Rhodopseudomonas capsulata, Bacillus licheniformis* or *Bacillus subtilis* (23). These microorganisms can be used in the synthesis of inorganic materials used, for example, as biological catalysts. They can aid in the mineralization or actively participate in bAuNPs synthesis (24). Bacteria can synthesize nanomaterials in culture medium in a given incubation period (extra or intracellularly), which renders the establishment of this approach as a flexible and reasonable method suiTable for large-scale production of NPs (21).

The biosynthesis of nanoparticles translates an upwards approach and involves the oxidation/reduction of metallic ions by biomolecules such as proteins, enzymes, carbohydrates, sugars, among others, secreted by microorganisms (25). A complete understanding of the biosynthesis of NPs by microorganisms are not yet noticeably clear, since each microbial organism uses different routes to interact with metallic ions. The synergy activities of a specific microorganism and the biochemical processing, as well as the effect of environmental conditions such as temperature and pH ultimately affect the size, shape, and morphology of the synthesized nanoparticles (26).

Among all applications, the potential of AuNPs as antitumoral and antibacterial agents has been exploited. These nanostructures have proven to have a great potential in these areas, increasing the need to improve synthesis methods, making them more profiTable and sustainable (15, 16, 27).

1.2 *Pseudomonas aeruginosa*

P. aeruginosa is being used as a reference strain of *P. aeruginosa* a Gram-negative, motile (with a single polar flagellum), bacillus (rod-shaped), nonspore-forming, facultative anaerobic (28), opportunistic pathogenic bacteria that belong to the Gammaproteobacteria class (29) and Pseudomonadaceae family (30, 31). This bacterial specie can grow in a temperature range of 5-42 ºC. In culture, show a blue-green appearance, due to the mixture of pyocyanin (blue/green) and pyoverdine (yellow/green) pigments (30).

P. aeruginosa occurs in both soil and aquatic environments, from abiotic to biotic environments, to plant and animal tissues. It can be isolated from various sources, including: several nosocomial and harmful infections, from the medical equipment, and from sinks and toilets (32).

Despite the pathogenicity of *P. aeruginosa*, several beneficial roles of this bacterium have also been explored in a variety of-field. This organism has the ability to produce a wide variety of compounds with bactericidal or bacteriostatic activity, including pyocyanin and other heterocyclic compounds such as quinolines, phenylpyrroles, and phenazines that may play advantageous roles in medicine (33). In the industries, *P. aeruginosa* beneficial roles are being explored for a diversity of applications, such as: oil refineries, waste degradation, textile products, pulp and paper, agriculture, mining, and explosive industries (34). Furthermore, the usage of herbicides and other products in the soils, as well as petroleum pollution, also open the possibility of its use for bioremediation and biodegradation (34).

In addition to all possible applications for *P. aeruginosa*, it has also been investigated for AuNPs production. Some studies have described the synthesis of AuNPs using this bacterium, for example Abd El-Aziz M. et. al reported the utilization of different *P. aeruginosa* strains for extracellular biosynthesis (using the supernatant) of AuNPs. When compared to AuNPs prepared by chemical methods, they noticed that one of the tested strains exhibited better yields. In addition, they also observed a relationship between the maximum absorption peak and the size of the AuNPs, and concluded that the extracellular synthesis is a simple and easier approach for downstream processing (35). Almost no studies have described the variation of AuNPs synthesis conditions in terms of culture preparation and physicochemical parameters, however, Timoszyk et al. have explored the green synthesis of AuNPs using *P. aeruginosa* with the variation of temperature and, reaction time, and have tested the antimicrobial activity towards *E. coli*. In this work, the authors noticed that secondary metabolites present in the

supernatant of *P. aeruginosa* were used as reducing agents. They observed that the smallest and spherical nanostructures were obtained at 25 ºC and the larger at 45 ºC. With the increase of temperature, the authors noticed an increase of size and a stability decrease. Moreover, a good antibacterial activity was shown for the synthesized AuNPs against *E. coli* indicating their potential in biological applications (36).

The biosynthesis mechanism of bAuNPs by *P. aeruginosa* is still unclear. However, Nangia et al. highlights a NADPH-dependent reductase enzyme that converts Au (III) to Au (0) through electron shuttle enzymatic metal reduction process in *Stenotrophomonas maltophilia,* a bacterium, that such as *P. aeruginosa*, belongs to Gammaproteobacteria class, suggesting a capping of bAuNPs by negatively charged phosphate ions from NADP (Figure 1.2) (37). In *P. aeruginosa* there are various genes encoding NADPH dependent enzymes which are related to oxidative stress and antimicrobial susceptibility. One of these is the glutathione-reductase-encoding gene (GR). In *E. coli*, glutathione (GSH) peroxidase reduces hydrogen peroxide to water and oxygen molecules, and the two molecules of GSH are oxidized to form GSH disulfide (GSSG). At high concentrations, GSSG is toxic and must be reduced back to GSH using electrons from NADPH by the GSH reductase. GSH reductase appears to have the same role in *P. aeruginosa* (38, 39).

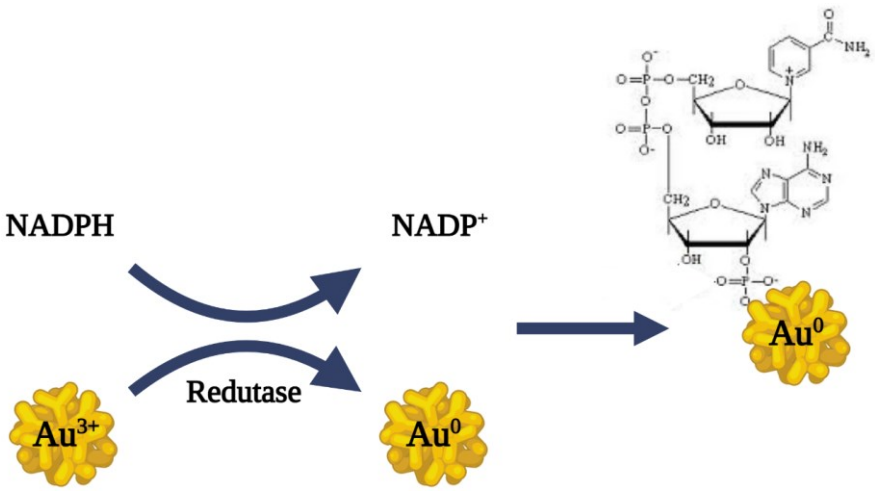

Figure 1.2 - Representation of the putative mechanism of bAuNPs synthesis proposed by Nangia et. al (37).

1.4 Prostate cancer and gold nanoparticles

According to the International Agency for Research on Cancer, prostate cancer (PCa) is estimated to have the highest worldwide incidence among men, with around 1,414,259 new cases in 2020 (40). In addition, even comparing to other cancers that affects both male and

female PCa continues to lead the Tables, becoming the fourth with the highest incidence (40). Nanotechnology has gained significant attention in administration and treatment of cancer globally, in a subdivision of nanomedicine called nanooncology (41).

There are three well accepted mechanisms proposed for the anticancer activity of AuNPs. In a firsthand AuNPs can interact with the cell membrane causing mitochondrial disfunction. The second mechanism is based on the apoptotic pathway induced by ROS (reactive oxygen species) instigating oxidative stress and, consequently leading to the DNA fragmentation in cancerous cells due to the elevated levels of ROS. Thirdly, AuNPs can interfere with the chemistry of proteins or DNA (42).

The inflammatory process has a significant role in PCa pathogenesis, by modulating tumor microenvironment (43, 44). This process involves the alteration of the balance of chemokines, cytokines, reactive oxygen species and transcriptional factors. Among them, the most extensively studied cytokine has been interleukin 6 (IL-6) which is well recognized as a prime regulator of PCa development (43-45).

Results obtained by Al-Trad B. et al. after administration of AuNPs on induced benign prostatic hyperplasia (BPH) in rats, suggests that AuNPs influence cancer inflammatory state. The authors observed that AuNPs reduce prostate IL-6 levels, and that this impact was more significant in smaller nanoparticles. (46). The study developed by Slepicka et al. showed that the active immunity against cancer cells is dependent on the charge of AuNPs, being the positive charged AuNPs more successful in the promotion of the anti-inflammatory effect, than the negative charged ones (47).

Various studies have reported the cytotoxic activity of AuNPs against normal and cancer cells dependent on the shape and size of the nanostructures. These factors exhibit an important role in terms of internalization, a mechanism that has been reported by many authors (48-50). Tarantola et al., reported that spherical AuNPs are more efficiently absorbed and more toxic than rod-shaped nanoparticles (48) and Wozniak et al. described the higher toxicity of the nanorods and nanospheres than flower, star, and prism shaped AuNPs in HeLa cell lines (49). Contrarily to these observations, the results obtained by Steckiewicz et al. reported a higher cytotoxicity for AuNPs stars against human bone osteosarcoma cell lines (50). The surface properties of AuNPs are also essential for the uptake and internalization in cells. The biomolecules localized on the AuNPs surface will influence nanomaterials toxicity and will dictate the interactions with the cellular membrane that can potentiate or not AuNPs

internalization (51-53). One of the proposed mechanisms for cellular uptake and internalization is based on the interaction of positive charges on the surface of AuNPs with the negative charges of phosphate groups on the lipids constituting the cellular membrane (44-46). Some authors have also described the entrance of AuNPs by endocytosis, reporting the uptake of small nanoparticles and their aggregation inside HeLa cells (54).

The concentration of AuNPs also influences cytotoxicity in healthy and cancer cell lines (55-58). However, due to the variety of shapes, sizes, and capping agents that can change nanoparticle functionality, as well as the variability of cell lines, opinions about AuNPs toxicity can vary significantly (59).

Prema et al. have tested the effect of green tea synthetized AuNPs in PC3 cells. The authors have concluded that these bAuNPs exhibit an anti-proliferative effect in PC3 cell lines and proposed the involvement of highly active biomolecules (60). In another study, Nambiar et al. assessed the interaction curcumin-coated AuNPs (cur-AuNPs) with PC3 cells grown in the presence of serum protein and in the absence of serum. In a serum free environment, the authors observed an interesting antitumoral effect, attributed to the accumulation of AuNPs in the cell surface. Contrarily, in the presence of serum protein, the effect decreased, with the authors hypothesizing that the adsorption of oppositely charged molecules in the serum may have changed the surface charge and chemistry of the cur-AuNPs, lowering their cytotoxicity (61).

1.5 Bacteria and gold nanoparticles

The unique physicochemical characteristics of AuNPs render their application as bactericidal agents has become an important research topic (62). The growing development of resistant strains of microbes caused by the misuse or over use of antimicrobials, such as antibiotics, antivirals, antifungals and anti-parasitic (63), has increased the necessity for the use of an agent presenting good antimicrobial properties and not causing resistance. AuNPs presents bactericidal properties against a variety of microorganisms, and their effect depends again, on size and shape (64).

1.5.1 Gram-negative bacteria

1.5.1.1 *Escherichia coli*

E. coli is a Gram-negative bacterium, rod-shaped (bacilli) that belongs to the Enterobacteriaceae family (65). *E. coli* is a commensal bacterium and is the most common Gram-negative bacteria in the gastro-intestinal tract of humans. When found in the intestinal tract *E. coli* lacks pathogenicity, however when located outside the intestine it can cause urinary tract infections (UTI), bacteremia, pneumonia, and peritonitis, among others (66-69). Cui et al., reported that AuNPs inhibited the growth of *E. coli* by collapsing the membrane potential, disrupting ATPase activity and inhibiting the binding of ribosome subunits to tRNA (70).

1.5.1.2 *Klebsiella pneumoniae*

K. pneumoniae also belongs to the Enterobacteriaceae family and is reported as a non-motile, encapsulate and Gram-negative bacterium. A wide array of factors provides virulence to this bacterium that can result in infection and antibiotic resistance. An important virulence factor is the polysaccharide capsule of the organism. Another virulence factors are the lipopolysaccharides that coat the outer surface of these Gram-negative bacteria and fimbriae, which allows the organism to attach itself to host cells (71-73). Aside from the virulence factors mentioned, *K. pneumoniae* is well-known for its ability to produce biofilms, which protect the bacteria from antibiotic diffusion and thus reduce their effects (74). Khosravi et al. tested bAuNPs coated with *Anthemis atropatana* extract against multidrug-resistant K. pneumoniae strains and found that the synthesized bAuNPs significantly inhibited biofilm formation in all biofilm-forming strains (75).

1.5.2 Gram-positive bacteria

1.5.2.1 *Staphylococcus aureus*

S. aureus is a non-motile, Gram-positive, coccoid bacterium of the Staphylococcaceae family. *S. aureus* is found in 20–40% of the general population human commensal microbiota of the nasal mucosa (76, 77). Soon after methicillin was introduced into clinical practice, Methicillin-resistant *S. aureus* (MRSA) was described in England in 1961 for the first time (78).

Although colonization at other sites can occur, particularly in the perineum and throat, the main site of *S. aureus* colonization is the nose (79). The uptake of staphylococcal cassette chromosome mec (SCCmec) via horizontal gene transfer (80), lead to *S. aureus* clones' development into MRSA. SCCmec is a mobile genetic element that encodes the genes mecA or mecC, which confer resistance to most β-lactam antibiotics, including methicillin. Current and future alternatives for *S. aureus* infections treatment are highly determined by the remarkable ability of this pathogen to acquire antibiotic resistance (81). In a study by Baker et al., the antibacterial activity and DNA-damaging properties of bAuNPs were tested against MRSA and found to have the ability to damage DNA, potentially contributing to their antimicrobial activity (82).

A variety of authors have described the antimicrobial effect of bAuNPs against a diversity of bacterial species, including Gram-negative and Gram-positive bacteria (83-86) (Table 1.1).

Table 1.2 - Brief literature revision of microbial strains treated with bAuNPs

Reference	Microbial species tested	Organism used in AuNPs synthesis	Outcomes of the antimicrobial study
Ahmad et al. (83)	*E. coli* and *S. aureus*	*Candida albicans* (cell free extract)	-Both species showed alterations in growth curves with lag phase extension; -Higher effect in *E. coli* then *S. aureus;* - Increasing effect with AuNPs concentration increase.
Folorunso et al. (84)	*S. aureus*, *Entrococcus faecalis*, *K. pneumonia*, *Clostridium sporogenes*.	*Annona muricata* (leaf extract)	- Increasing effect with AuNPs concentration increase; - The order of potency of AuNPs was: *S. aureus* > *Entrococcus faecalis* > *K. Pneumonia* > *Clostridium sporogenes*.
Abdel-Raouf et al. (85)	*E. coli*, *K. pneumoniae* MRSA, *S. aureus* and *P. aeruginosa*	*Galaxaura elongata* (powder and ethanolic extract)	- The order of potency of ethanolic extract AuNPs was *E. coli* > *K. pneumoniae* > MRSA > *S. aureus* > *P. aeruginosa*; -AuNPs synthesized by the powder were highly effective

			against E. coli and K. pneumoniae.
Geethalakshmi et al. (86)	*S. aureus*, *Streptococcus faecalis*, *Enterococcus faecalis*, *E. coli*, *P. aeruginosa*, *Proteus vulgaris*, *Bacillus subtilis*, *Yersinia enterocolitica*, and *Candida albicans*	*Trianthema decandra* (Plant exctract)	-Nanoparticles showed excellent activity against *Yersinia enterocolitica*, *Proteus vulgaris*, *E. coli*, *S. aureus*, and *Streptococcus faecalis;* -Nanoparticles tested were more effective in Gram-negative bacteria; - Small nanoparticles presented higher antimicrobial effects.

The mechanisms underlying AuNPs antibacterial activity are not well understood. However, Abdel-Raouf et al. suggested that AuNPs mechanism of action may be similar to that of silver nanoparticles (AgNPs). The authors refer a disruption of the DNA replication and ATP production by the uptake of free silver ions; followed by an increase of the oxidative stress by the formation of Reactive Oxygen species (ROS) that prompts a cell damage caused by the direct interaction with the cellular membranes (85).

1.7 Work relevance

The significance of this study stems from its goal of improving a simple and cost-effective method for synthesizing tuned green gold nanoparticles using PAO1, a bacterium known to produce a variety of bioactive compounds. Thus, the primary objectives of the study are:

O1: To determine the most effective culture conditions for synthesizing bAuNPs using PAO1;

O2: To observe how pH, temperature, and incubation time affect the synthesis, shape, size, and aggregation of the bAuNPs;

O3: To examine how the tunning of bAuNPs, affects its potential as antitumoral and antimicrobial agents.

In addition to the main objectives, this work addresses two hypotheses, the first is based on the the possibility of using DCIP as an indicator of the reducing potential of PAO1 for the synthesis of bAuNPs. The other hypothesis proposes the possible involvement of GSH reductase in the synthesis of bAuNPs.

This study aims to fill the gap in our knowledge of bAuNPs synthesized using *P. aeruginosa* and has the potential to contribute significantly to the development of new and effective treatments for prostate cancer and for bacterial infections.

2. Methodology

2.1 AuNP biosynthesis - Optimization and Characterization

2.1.1 *Pseudomonas aeruginosa* strain and maintenance

Pseudomonas aeruginosa (PAO1, ATCC 15692) was isolated and maintained at Laboratory of Medical and Industrial biotechnology (LaBMI), Porto Research, Technology & Innovation Center (PORTIC), Porto, Portugal. Bacteria were routinely cultured in Trypticase soy agar (TSA) plates where the fluorescent pigment pyoverdine typically produced by PAO1 strains was observed.

2.1.2 Optimization of the bacterial growth conditions for maximum reduction potential

DCIP (Sigma-Aldrich, Merck KGaA, Missouri, USA) is a compound that can be directly reduced by NAPH being the final reaction products two-electron reduced forms of DCIP and NADP+ (2.1; Eq. 1) (87) with a change of color from blue to red, easily denoted by an absorbance decay at 600 nm (OD_{600}). Bearing in mind that NADPH may be involved in the synthesis of nanoparticles by interacting with reductases, DCIP is suggested as an indicator of PAO1 reduction potential (Fig. 2.1). Experiments were conducted to determine at which optical densities (OD) of the bacterium the absorbance decay of DCIP is most pronounced over time, and to compare the efficiency of the bacteria extract in the synthesis of bAuNPs.

$$\mathbf{DCIP}_{oxi} + \mathbf{NADPH} \rightarrow \mathbf{DCIP}_{red} + \mathbf{NADP^+} \qquad (2.1;\ Eq.\ 1)$$

Isolated colonies of PAO1 were cultured in Tryptic Soy Broth (TSB) at the following optical densities (OD_{600}): 0.1, 0.2, 0.5, 1, 1.5 and 2.0 at 37 ºC. Each culture was centrifuged for 10 min at 4000 rpm. The supernatant was recovered, and DCIP (20 mg/mL) was added, being the absorbance decay measured by spectrophotometry at 600 nm (OD_{600}) after 24 h. The process was repeated with a time interval of 3 h during 24 h of culture growth. A kinetic measurement of PAO1 culture in the same OD was run in parallel for a 24 h period at 37 ºC with a time interval of 30 minutes and with no DCIP addition. All measurements were carried out in triplicate. The same experiment was repeated at the higher temperature at which PAO1 can grow (42 ºC), to investigate the effect of temperature stress on the reduction potential of PAO1 cultures (Appendix 1).

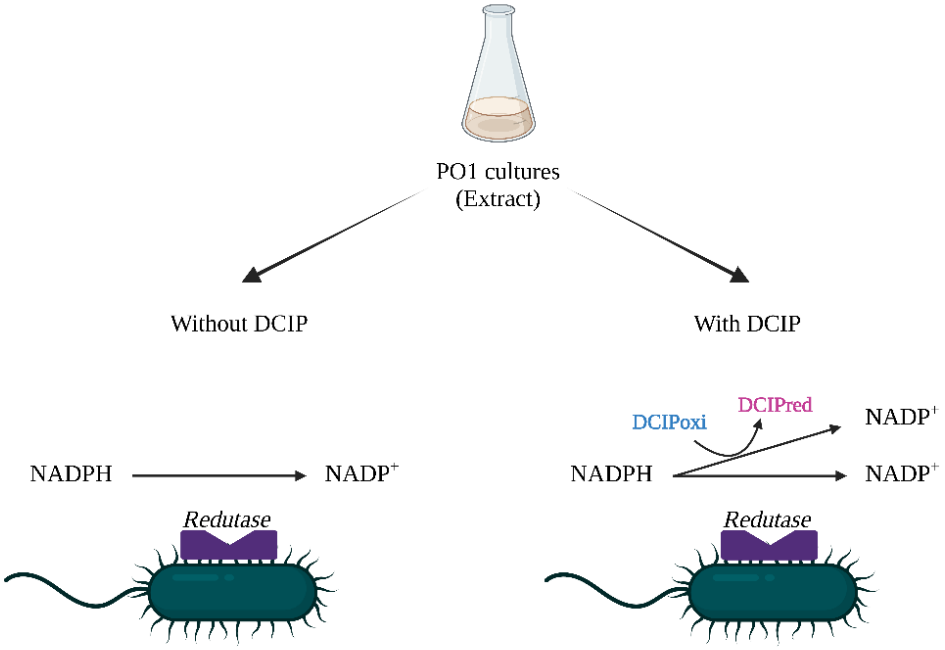

Figure 2.1 - Putative mechanism for the proposed DCIP method; On the left is represented NAPH dependent reductase present in PAO1 extract without the addition of DCIP; On the right is represented an alternative route for NADPH molecule in PAO1 extract being oxidized and reducing DCIP from blue to red.

2.1.3 Confirmation of DCIP method as an indicator of PAO1 reduction potential and investigation of GR gene possible involvement in AuNPs biosynthesis

To confirm the hypothesis of DCIP as an indicator of PAO1 reduction potential in bAuNPs biosynthesis, the optical density was adjusted to 1.0 (OD_{600}) and the culture was grown in 100 mL of TSB at 37 ºC. Cultures were maintained at 150 rpm. The supernatant was

recovered by centrifugation at 4000 rpm for 10 min at four different culture times: 0, 9 and 19 h. After, a solution of chloroauric acid ($HAuCl_4$, 50 mM) (Sigma-Aldrich, Merck KGaA, Missouri, USA) was mixed with the cell free supernatant. The pH was kept at 9.0 by using a NaOH solution (0.1 M). All solutions were done in triplicate and maintained at 50ºC for 24h. Following that, a PAO1 strain with a deletion in the GR gene (mutant), was employed to investigate the possible involvement of GSH reductase in the biosynthesis of AuNPs. This mutant was also grown in 100 mL of TSB for 37 ºC and kept under stirring at 150 rpm. The supernatant was recovered at 9 h. Again, a solution of $HAuCl_4$ (50 mM) was added to the cell free supernatant and the pH was adjusted to 9.0 with NaOH (0.1 M) solution. The reaction was performed in triplicate at 50 ºC for 24 h. Together with the experimental tubes, solutions also subjected to the same pH adjustment but without the addition of chloroauric acid were used as control.

2.1.4 Biosynthesis of AuNP at different physicochemical conditions

To evaluate the effect of different physicochemical parameters, the biosynthesis of bAuNPs was carried out under different reaction conditions. PAO1 was again cultured at OD_{600} = 0.1 in 100 mL TSB and maintained at 150 rpm for 9 h. The supernatant was recovered by centrifugation at 4000 rpm. After, a HAuCl4 solution (50 mM) was mixed with the cell free supernatant.

Effect of pH in the bAuNPs synthesis - The pH of the cell free extract was varied at 5.0, 6.0, 7.0, 8.0, and 9.0 at different reaction temperatures (29, 37, 50, and 58 °C) and different reaction times (24, 48, and 72 h) by adding 0.1M HCl or 0.1M NaOH until reach the required pH.

Effect of reaction temperature and time in the bAuNPs synthesis - The reaction mixtures obtained by varying the pH were maintained in the experimental tubes and incubated in a rotary shaker at 150 rpm for varied time intervals of 24, 48, and 72 h at different reaction temperatures (29, 37, 50, and 58 °C).

Control solutions (without the addition of HAuCl4) were also run along with the experimental tubes and subjected to the same reaction conditions. Sample identity (ID) indicates the physicochemical parameters for the synthesis of bAuNPs. For example, in sample ID

GNP9.24.58, GNP indicates gold nanoparticles, 9 indicates pH 9.0, 24 indicates reaction time in hours and 58 indicates incubation temperature.

2.1.4.1 Characterization of biosynthesized bAuNPs

2.1.4.1.1 UV-Visible Spectroscopy (UV-Vis)

To confirm the presence of AuNPs, the excitation spectra of the samples were measured by UV-Vis using the Multiskan SkyHigh spectrophotometer (Thermo Fisher Scientific, Massachusetts, USA). The pellets of control and AuNPs solutions were resuspended in DEPC-treated water (Thermo Fisher Scientific, Massachusetts, USA), mixed by vortex, and the excitation spectra were recorded in a wavelength range of 300 to 700 nm. All measurements were done in a quartz cuvette (1mm). Concentrations of gold ions that were reduced to AuNPs in the biosynthesis process were calculated following Scarabelli et al. (88) correlation, where, from the absorbance at 400 nm and for a 1 mm cuvette, an absorbance of 1.2 (OD_{400}) corresponds to [Au^0] = 0.5 mM:

$$\frac{1.2}{A\ 400\ nm} = \frac{0.5\ mM}{x} \qquad \text{(2.1; Eq. 2)}$$

Also, UV-Vis data was used to obtain the aggregation values as described by Ye et al. (12). The ratio between the absorbance at 650 nm (aggregated AuNPs) and the absorbance at 530 nm (dispersed AuNPs) was used to express the molar ratio of aggregated to dispersed AuNPs:

$$Agregation = \frac{A\ 650\ nm}{A\ 530\ nm} \qquad \text{(2.1; Eq. 3)}$$

2.1.4.1.2 Transmission Electron Microscopy (TEM)

10 µL of each sample was mounted on carbon film-coated mesh nickel grids and left standing for 2 min. The excess liquid was removed with filter paper from all samples, and the grids were observed in a JEM 1400 TEM (JOEL Ltd., Tokyo, Japan) with an accelerating voltage of 80 kV. Images were digitally recorded using a CCD digital camera (Orious 1100W Tokyo, Japan). After, images were analyzed using ImageJ (U. S. National Institutes of Health, Bethesda, USA) software to assess the mean particle size.

2.1.4.1.3 Attenuated Total Reflection Fourier-Transform Infrared Spectroscopy (ATR-FT-IR)

The gold nanoparticles presenting higher yields (GNP9.24.50, GNP8.24.50 and GNP9.24.58) were subjected to ATR-FT-IR analysis. The ATR-FT-IR analyses were performed using the Frontier™ MIR/FIR spectrometer (PerkinElmer, Massachusetts, USA) in a scanning range of 550–4000 cm^{-1} for 16 scans at a spectral resolution of 4 cm^{-1}.

2.2 bAuNP against prostate cancer

In the following subsections of this work, are presented the methods for prelaminar screening of the bAuNPs activity on prostate cell carcinoma. To study the effects of the bAuNPs, two different cell models were used: the neoplastic prostate cell line PC3, which is derived from a cancerous prostate tissue, and the normal epithelial cell line HPEpiC, which is derived from healthy prostate tissue. In order to evaluate the activity of the bAuNPs, a series of *In vitro* assays were performed, including assessments of cell viability, proliferation, migration, and IL-6 levels. GNP9.24.50, GNP8.24.50, and GNP9.24.58 were tested. These bAuNPs conditions were chosen due to their consistently high synthesis yields during the synthesis process.

2.2.1 Cytotoxic effect evaluation of the bAuNPs in prostate cell lines

2.2.1.1 Cell culture and treatments

PC3 and HPEpiC were seeded in RPMI 1640 medium (VWR, Biowest, P0860-N10L, USA) supplemented with 10% of Fetal Bovine Serum (FBS, Gibco, Life technologies, 10270, USA) and 1% penicillin/streptomycin (Gibco, Life technologies, 10270, USA). The cells were maintained at 37 °C in a humidified chamber containing 5% CO_2. Treatments were performed using three different bAuNPs: GNP9.24.50, GNP8.24.50 and GNP9.24.58, at a final concentration range of 0.5-10^{-4} mM and the dilutions were made using the serial dilution method, being the serum free cell culture medium, the solvent used. GNP9.24.58 at 10^{-3} mM

final concentration, was the only condition used in the cellular uptake, injury, and IL-6 ELISA assays.

2.2.1.2 bAuNPs cellular uptake assay

Fluorescence microscopy was used for qualitative examination of the uptake of rhodamine B fluorescent-labeled bAuNPs by PC3 cell lines. In the of bAuNPs suspension, the rhodamine B (RhoD) solution was added followed by stirring for 24 h at 25 ºC in a dark room. Then, RhoD-loaded bAuNPs were recovered by centrifugation at 5000 rpm for 10 min. The cells were grown in cover slips and treated with Rhodamin B-loaded bAuNPs and non-treated cells used as control. After 24 h the cells were washed with Phosphate buffered saline (PBS). Finally, nuclei were marked with 4′,6-diamidino-2-phenylindole (DAPI). Before analysis, cells were fixed using paraformaldehyde (3,7%), followed by three washing steps. After the washing steps, 300 µL of DAPI (10 ng/mL, Thermo Fisher Scientific, USA) was added and the culture was incubated for 10 min at 25 ºC. Rhodamine B-labelled bAuNPs uptakes were observed using a fluorescence microscope (EVOS M7000 microscope, Thermo Fisher Scientific, USA).

2.2.1.3 Viability assay

The 3-[4,5-dimethylthiazol-2-yl]-2,5 diphenyl tetrazolium bromide (MTT) assay (Life Technologies, Thermo Fisher Scientific, USA) was carried out following the manufacturer's instruction. In brief, 1.0×10^5 cells/mL (PC3) or 2.5×10^5 cells/mL (HPEpiC) were seeded in a 96-well plate and grown until 80% confluence. Each bAuNPs were incubated for 24 h in cell culture. After the washing step with warm PBS, 0.5 mg/mL of MTT was incubated for 2 h at 37 °C. The absorbance was then measured with a microplate reader at 570 nm (Multiskan SkyHigh, Thermo Fisher Scientific, Massachusetts, USA).

2.2.1.4 Proliferation assay

The proliferative potential of the cells was evaluated using the Roche Diagnostics BrdU kit, which was carried for the colorimetric bromodeoxyuridine (BrdU) assay (Rotkreut, Switzerland). Briefly, PC3 (1.0×10^5 cells/mL) and HPEpiC (2.5×10^5 cells/mL) were seeded into a 96-well flat-bottomed tissue culture plate until reaches 80% confluence. The cell culture

was seeded with 0.01 mM BrdU for 24 h during the treatment period with bAuNPs. After binding to the BrdU integrated into the newly synthesized DNA using an antibody-bromodeoxyuridine-peroxidase (anti-BrdU-POD) solution, the supernatant was removed, and the wells were rinsed three times with a 1x washing solution. The substrate solution was incubated in the dark at room temperature for 10 min to detect immune complexes. The reaction product was quantified by measuring the absorbance at 660nm using a microplate reader (Multiskan SkyHigh, Thermo Fisher Scientific, Massachusetts, USA).

2.2.1.5 Injury assay

PC3 (4.0 x 10^5 cells/mL) and HPEpiC (6.0 x 10^5 cells/well) cells were seeded into a 6-well flat-bottomed tissue culture plate and grown to confluence before being injured with a pipette tip (200 µL). Following that, the bAuNPs were added to the cultures, and the wounded cell monolayer was photographed with an inverted microscope at a magnification of 10x (Nikon Instruments Inc., Melville, USA). The migration distance was scanned 24 h after treatment, and the scratch closure was determined using Image J (U. S. National Institutes of Health, Bethesda, USA) software by measuring the damage width.

2.2.1.6 Human interleukin 6 (IL-6) ELISA assay

The detection and quantification of IL-6 were done using a solid-phase sandwich Enzyme-Linked Immunosorbent Assay (ELISA). Firstly, PC3 (4.0 x 105 cells/mL) and HPEpiC (6.0 x 105 cells/well) cells were seeded into a 6-well flat-bottomed tissue culture plate and grown to confluence, followed by the addition of GNP9.24.58 (10^{-3} mM final concentration), being the culture medium collected after 24 h. The supernatant was used to perform the ELISA assay (Invitrogen, Thermo Fisher Scientific, USA), following the manufactures instructions. In brief, 100 µL of the sample (culture medium) and 50 µL of the Hu IL-6 Biotin Conjugate solution were added to each well of 98 well plate. After 2h of incubation, the solution was removed, and each well was washed 4 times with 1x washing solution. After 2 h of incubation, the solution was removed and 100 µL of 1x Streptavidin-HRP solution was added and incubated for 30 min, the solution was then removed, and wells were washed 4 times. Subsequently, stabilized chromogen was added to each well and

incubated for 30 min at room temperature in the dark. Finally, 100 µL Stop Solution was added and absorbance was measured at 450 nm.

2.3 AuNPs against Gram-positive and Gram-negative bacteria

The methods used for prelaminar screening of the activity of bAuNPs on the growth (kinetics) and viability of bacteria are described in the following subsections. The effects of bAuNPs were studied using two Gram-negative bacteria and one Gram-positive bacterium. GNP9.24.50, GNP8.24.50, and GNP9.24.58 were the only bAuNPs conditions tested. These bAuNPs conditions were chosen due to their consistently high synthesis yields during the synthesis process.

2.3.1 AuNPs effect on bacteria growth – Kinetics

The influence of gold nanoparticles in the kinetics growth curve was tested on three bacteria: two Gram-negative bacteria (namely, *K. pneumoniae* ATCC 13893 and *E. coli* ATCC 22953) and one Gram-positive bacterium *S. aureus*. Two strains of S. aureus were used. For the present study it was used (a methicillin-resistant *S. aureus* (MRSA, ATCC 43300) and a methicillin-susceptible *S. aureus* (MSSA, ATCC 25923). All strains were cultured in Muller-Hinton Broth (MHB) and adjusted to 0.1 optical density. Three AuNPs were tested against the bacteria: GNP8.24.50, GNP9.24.50 and GNP9.24.58. The effect of AuNPs in bacterial growth was performed by the serial dilution method, with final concentrations of the bAuNPs ranging from 0.5 to 10^{-4} mM. Cultures were grown together with AuNPs in 96 well plates adding 100 µL of the final solution in each well and maintaining at 37 ºC for 24 h. Absorbances (OD_{600}) were measured every 30 minutes using the Multiskan SkyHigh spectrophotometer (Thermo Fisher Scientific, Massachusetts, USA) over a 24 h period. Control wells containing only medium, and bacteria were monitored in the same conditions throughout the experiment.

The area under the curve (AUC) was calculated using GraphPad prism 9.0.0 (GraphPad Software, Inc., USA), which was used as cumulative measure of the effect of the AuNPs in the total growth of bacteria. To understand the differences to the control, the relative growth was obtained as the quotient (percentage) of the AUC of bacteria with bAuNPs (test) divided by the AUC of bacteria without bAuNPs (control):

$$Relative\ growth = \frac{\int_{x_0}^{x} f(x)_{test}}{\int_{x_0}^{x} c(x)_{control}} \times 100\% \qquad (2.1;\ Eq.4)$$

2.3.2 AuNPs effect on the viability of *E. coli* and MRSA

The effect of AuNPs in the viability of E. coli and MRSA was evaluated by counting the number colonies formed in Muller-Hinton Agar (MHA) plates after 24 h growth at 37 ºC. For that, the initial concentration of bacteria was firstly adjusted to 0.1 of optical density (OD_{600}) in MHB and GNP9.24.50 was added in the culture in a final concentration of 10^{-1} mM. After growth at 37 ºC for 24 h, the treated cultures were submitted to a serial dilution from 10^{-1} to 10^{-8} and 20 µL of each solution was plated in triplicate in MHA plates. Control solutions (without addition of bAuNPs but subjected to the same serial dilutions) were also plated in MHA plates and grown together with the test solutions. All cultures were grown at 37 ºC for 24 h in triplicate and the colonies were counted in a magnifying glass. After, CFU/ml was calculated using the following equation:

$$\frac{CFU}{ml} = \frac{Nº\ of\ colonies}{Volume\ of\ culture\ plated\ (mL)} \times dilution \qquad (2.1;\ Eq.\ 5)$$

Where, CFU/mL is the number of colony-forming units per milliliter; Nº of colonies is the number of colonies on the culture plate; Volume of culture plated (mL) is the volume of the culture that was plated on the plate, measured in milliliters and dilution is the dilution factor used when plating the culture.

2.4 Statistics analysis

All data was analyzed as the mean ± standard deviation (SD). All the assays were repeated in triplicate for statistical analysis. The statistical significance was determined using Student *t* test, 1-way analysis of variance analysis. Results were considered significant when *p<0.05, **p<0.01, ***p<0.001 and ****p<0.0001. All analysis were performed in GraphPad prism version 9.0.0 (GraphPad Software, Inc., USA).

3. Results

3.1 Optimization of the bacterial growth conditions for maximum reduction potential

3.1.1 DCIP Method

Different profiles of DCIP reduction were observed among all culture optical densities tested (OD_{600} = 0.1; 0.2; 0.5; 1.0; 1.5 and 2.0). Among the optical densities studied, it was observed a surprising absorbance decay for the optical density OD_{600} = 1.0 at 37 ºC. At all optical densities, bacteria have presented the highest reduction potential of DCIP during the late exponential growth phase. Absorbance decay of DCIP showed to increase with the increasing optical density of the culture, up to optical density OD_{600} = 1.0, starting to decrease thereafter (Fig. 3.1D). For cultures grown at 42 ºC the higher DCIP absorbance decay was obtained at optical density OD_{600} = 0.1, however, in all optical densities tested, the absorbance decay was inferior when compared to cultures grown at 37ºC (Appendix 1).

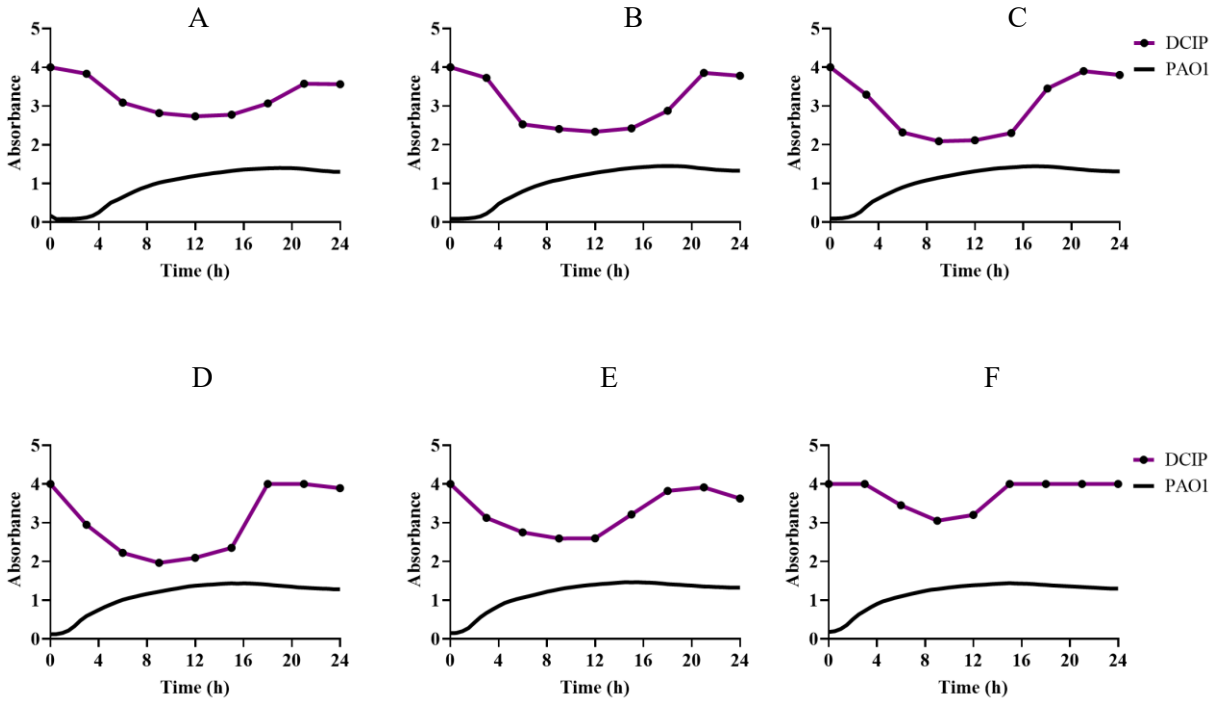

Figure 3.1 - Growth curve of PAO1 (black curve) cultured at different optical densities [A (OD = 0.1); B (OD = 0.2); C (OD = 0.5); D (OD = 1.0); E (OD = 1.5); F (OD = 2.0)] and the corresponding supernatant collected at specific times and where DCIP was added (black dots on purple curve).

3.1.2 Confirmation of DCIP method as an indicator of PAO1 reduction potential and investigation of GR gene possible involvement in AuNPs biosynthesis

To confirm DCIP method as an indicator of PAO1 reduction potential bAuNPs were synthesized with 0, 9 and 19 h culture extract. UV-vis spectra analysis allows to observe that 9 h culture extract has presented the higher yield (0, 39 mM), while the culture extracts obtained at 0 and 19 h have presented lower yields (0, 32 mM and 0,37 mM) (Figure 3.2).

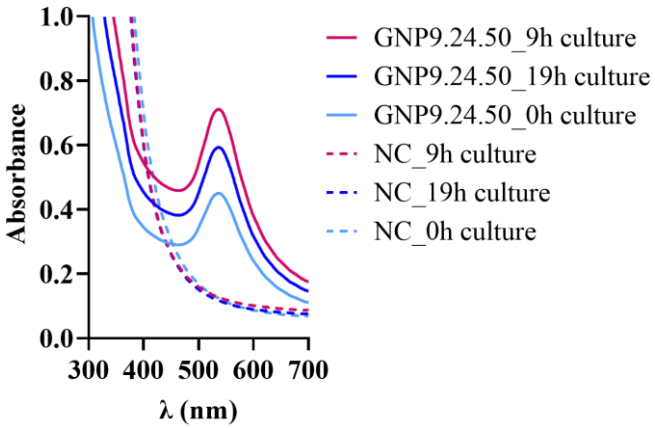

Figure 3.2 - UV-Vis spectra obtained for bAuNPs synthesized at pH 9 for 24 h at 50ºC with PAO1 supernatant collected after 0, 9 and 19 h of culture growth and the respective negative control (NC).

A mutated strain of PAO1 was used as a way of investigating the possible involvement of GSH reductase in the mechanism of biosynthesis of bAuNPs. As shown in Figure 2.4 the deletion of GR gene led to a reduction to a reduction of DCIP absorbance decay (Fig. 3.3A) and to a reduction of AuNP synthesis yield from 0,39 mM to 0,31 mM (fig. 3.3B).

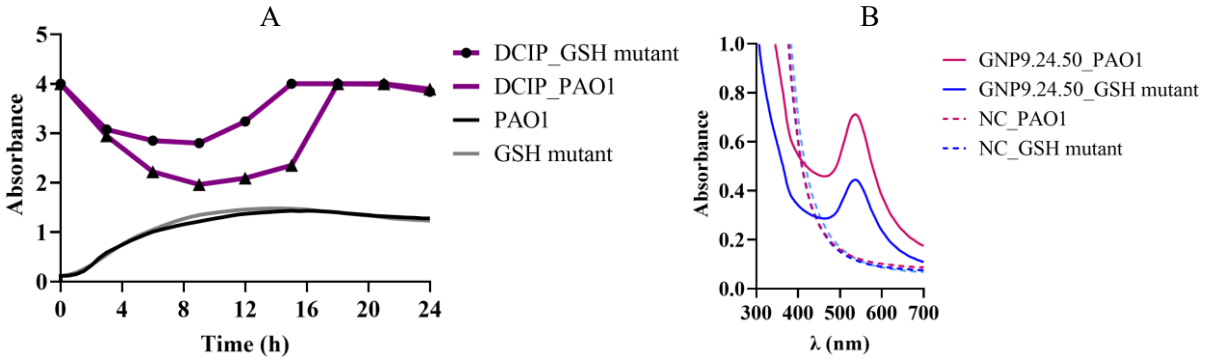

Figure 3.3 – (A) PAO1 wild type and GSH mutant growth and the corresponding supernatant collected at specific times with DCIP addition for PAO1 (black dots in purple curve) and for GSH mutant (black triangles in purple curve); UV-Vis spectra of bAuNPs synthetized at pH 9.0 for 24 h at 58 ºC with PAO1 and GSH mutant supernatant and the respective negative control (NC).

3.1.3 Biosynthesis and characterization of AuNPs

Varying a wide range of physicochemical parameters during the reaction process (i.e pH, time, and temperature), it was possible to observe different patterns in the biosynthesis AuNPs using PAO1. The synthesis of AuNPs became evident by the color change of the reaction solution, presenting colors ranging from red/pink to purple/blue tones, except for the biosynthesis at pH 5 and 6 that demonstrate to result in light-yellow/transparent solutions (Fig. 3.4).

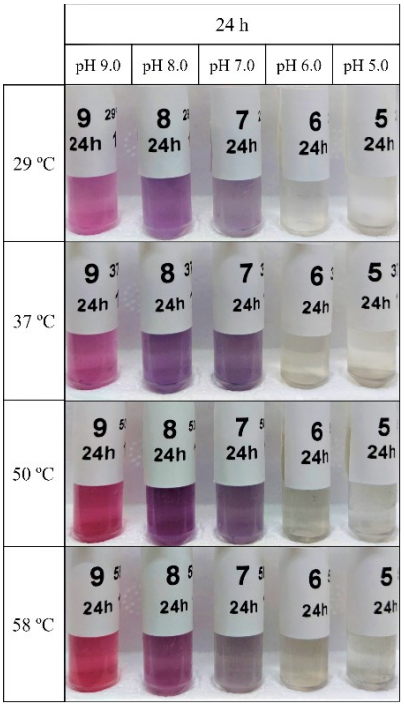

Figure 3.4 – Resulting bAuNPs colloidal solutions synthetized at different pH's and temperatures.

The synthesis of the bAuNPs was confirmed by UV-Vis, which revealed characteristic peaks in the 500-600 nm wavelength range. UV-Vis spectrometry was used to determine the concentration and aggregation of bAuNPs. The morphological features (shape and size) were obtained using TEM, and the functional groups were determined using ATR-FT-IR. The effects of pH, time and temperature in the aggregation, concentration, and size on the synthesis of bAuNPs, are presented in the following Table 3.1.

Table 3.1 - Effect of different physicochemical parameters on the biosynthesis of bAuNPs.

	pH	Time (h)	Temp. (C°)	Agreggation (650/530 nm)	Concent. (mM)	TEM size (nm)
Effect of pH						
GNP9.24.58	9.0	24	58	0.23	0.38	30.862 ± 13.48
GNP8.24.58	8.0	24	58	0.44	0.30	48.791 ± 22.66
GNP7.24.58	7.0	24	58	0.72	0.22	67.858 ± 33.49
GNP6.24.58	6.0	24	58	0.99	0.14	112.076 ± 26.75
GNP5.24.58	5.0	24	58	0.99	0.17	142.076 ± 34.24
Effect of pH and time						
GNP9.24.58	9.0	24	58	0.23	0.38	30.862 ± 13.48
GNP9.48.58	9.0	48	58	0.29	0.34	35.264 ± 13.48
GNP9.72.58	9.0	72	58	0.32	0.32	29.664 ± 12.21
GNP8.24.58	8.0	24	58	0.44	0.30	48.791 ± 22.66
GNP8.48.58	8.0	48	58	0.52	0.24	58.606 ± 23.88
GNP8.72.58	8.0	72	58	0.61	0.17	47.340 ± 24.71
GNP7.24.58	7.0	24	58	0.72	0.19	63.233 ± 33.49
GNP7.48.58	7.0	48	58	0.80	0.16	63.532 ± 34.63
GNP7.72.58	7.0	72	58	0.85	0.18	63.942 ± 30.59
GNP6.24.58	6.0	24	58	0.99	0.14	112.076 ± 26.75
GNP6.48.58	6.0	48	58	0.99	0.21	112.428 ± 33.32
GNP6.72.58	6.0	72	58	0.97	0.22	112.501 ± 32.39
GNP5.24.58	5.0	24	58	0.99	0.17	142.076 ± 34.24
GNP5.48.58	5.0	48	58	1,00	0.22	142.82 ± 28.86
GNP5.72.58	5.0	72	58	1,00	0.24	142.88 ± 29.49
Effect of pH and temperature						
GNP9.24.29	9.0	24	29	0.50	0.18	56.342 ± 12.92
GNP9.24.37	9.0	24	37	0.47	0.24	47.811 ± 16.01
GNP9.24.50	9.0	24	50	0.33	0.39	42.063 ± 16.86
GNP9.24.58	9.0	24	58	0.23	0.38	30.862 ± 13.48
GNP8.24.29	8.0	24	29	0.84	0.20	75.854 ± 11.85
GNP8.24.37	8.0	24	37	0.88	0.24	73.300 ± 16.01
GNP8.24.50	8.0	24	50	0.49	0.36	54.894 ± 35.50
GNP8.24.58	8.0	24	58	0.44	0.30	48.791 ± 22.66
GNP7.24.29	7.0	24	29	0.82	0.17	88.072 ± 20.91
GNP7.24.37	7.0	24	37	0.81	0.26	87.296 ± 22.78
GNP7.24.50	7.0	24	50	0.80	0.24	76.481 ± 32.92
GNP7.24.58	7.0	24	58	0.72	0.22	67.858 ± 33.49
GNP6.24.29	6.0	24	29	0.96	0.05	124.816 ± 28.53
GNP6.24.37	6.0	24	37	0.97	0.06	122.386 ± 56.61
GNP6.24.50	6.0	24	50	1.00	0.15	120.141 ± 44.45
GNP6.24.58	6.0	24	58	1.01	0.14	112.077 ± 26.75
GNP5.24.29	5.0	24	29	0.95	0.08	154.172 ± 37.56
GNP5.24.37	5.0	24	37	0.94	0.08	145.926 ± 31.49
GNP5.24.50	5.0	24	50	0.97	0.12	144.814 ± 36.36
GNP5.24.58	5.0	24	58	1.00	0.17	142.076 ± 34.24

3.1.3.1 Effect of pH on bAuNP synthesis

In order to study the effect of the pH on the biosynthesis of gold nanoparticles a pH range between acid, neutral and alkaline (pH = 5.0, 6.0, 7.0, 8.0 and 9.0) was tested. Among the conditions studied, it was primarily observed, by UV-vis spectroscopy a very slight surface plasmon signal (SPS) at pH 5 and 6 (GNP5.24.58 and GNP6.24.58) (Fig. 3.5), showing also very low bAuNPs concentrations (0.17 mM and 0.14 mM, respectively) and high aggregation values (0.99) (Table 3.1). However, the TEM analysis enabled the visualization of some

nanostructures, that revealed to be large (142.076 ± 34.24 nm and 112.076 ± 26.75 nm) (Table 3.1) and raspberry shaped (Fig. 3.6). At pH 7.0 (GNP7.24.58) the obtained concentration remained low (0.22 mM) (Table 3.1), being observed a broad and slight peak in the UV-Vis spectrum (Fig. 3.5). Again, predominantly raspberry shaped nanostructures were observed, with sizes of about 67.858 ± 33.49 nm (Table 3.1). The data obtained showed that the pH increase lead to narrower and more intense peaks in the UV-Vis spectrum. At pH 8.0 (GNP8.24.58), mixed shaped nanoparticles populations were found (raspberry to irregular shape), with a decrease of particle size (48.791 ± 2.66 nm), which turns even smaller at pH 9.0 [GNP9.24.58) (30,862 ± 13.48 nm)] (Table 3.1) where the spherical shape is predominant (Figure 2.7). The relationship between pH and the product yield became evident, being observed a yield increase (concentration increase) with the increase of pH (0.30 mM and 0.38 mM) for the pH values of 8.0 and 9.0, respectively (Table 3.1).

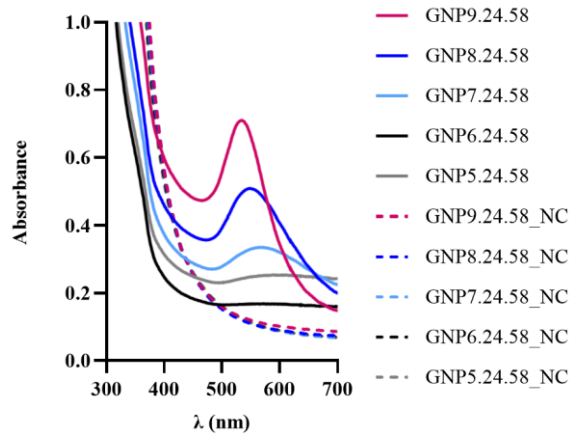

Figure 3.5 – UV-Vis spectra obtained for bAuNPs synthesized at different pH for 24 h at 58 ºC and the respective negative control (NC);

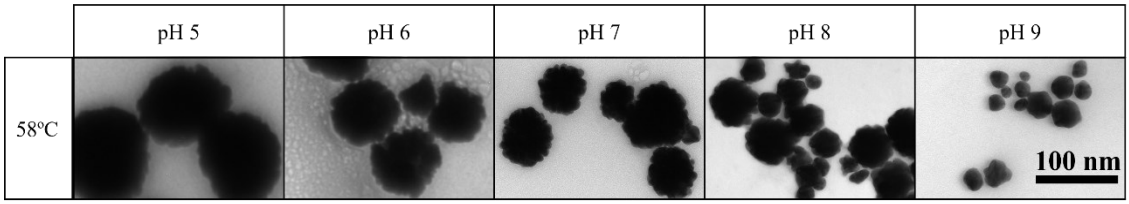

Figure 3.6 - TEM photographs of each bAuNP synthesized at different pH for 24 h at 58 ºC (100 nm ampliation).

3.1.3.2 Effect of time on bAuNP synthesis

The biosynthesis of bAuNPs was performed at different reaction times 24 h, 48 h and 72 h in order to address the influence of time on the products' yields, morphology and

aggregation. After 24 h at pH 9.0 (GNP9.24.58) the particles synthetized were primarily small spheres (30.862 ± 13.48 nm), but as time progresses, a growth of the particles at 48 h [GNP9.48.58 (35.264 ± 13.48)] was observed. However, at 72 h time-point (GNP9.72.58) particle size suffered a rupture in this trend, becoming smaller (29.664 ± 12.21 nm), but maintaining spherical shape at all time-points (Table 3.1 and Fig. 3.8). As the reaction time increased, was noticed that the concentration of nanoparticles decreases [GNP9.24.58 (0.32 mM) to GNP9.72.58 (0.30 mM)], being accompanied by an increase in particle aggregation, which remains, however, below 0.4 at all-time intervals (Table 3.1). Similarity, at pH 8.0 the trend of particle growth is maintained after 24 h and 48 h [GNP8.24.58 (48.791 ± 22.66 nm) and GNP8.48.58 (58.606 ± 23.88 nm)] (Table 3.1). Regarding shape, firstly, bAuNPs showed a raspberry shape, but after 72 h, bAuNPs started to take spherical shape (Fig. 3.8) accompanied by a slight decrease in size [GNP8.72.58 (47.340 ± 24.71 nm)] (Table 3.1). At pH 8.0 the concentration decreases with evolution of time [GNP8.24.58 (0.30 mM) to GNP8.72.58 (0.17 mM)] and, contrarily, aggregation increases [(GNP8.24.58 (0.44) to GNP8.72.58 (0.61)]. The UV-Vis spectra analysis showed a lowering of the peak intensities with time, for pH 9.0 and 8.0 (Fig. 3.7). At neutral pH 7.0 a lowering of the peak intensity was observed after 48 h (GNP7.48.58) (Fig. 3.7B) which remains after 72 h (GNP7.72.58) (Fig. 3.7C). A slight increase of concentration from 48 h (0.16 mM) to 72 h (0.18 mM) and aggregation from 24 h (0.72) to 72 h (0.85) was also noticed (Table 3.1). The raspberry shape remained at all time intervals, although, with larger spikes in the outer layer, approaching the star shape at 72 h (GNP7.72.58) (Fig. 3.8). At pH 6 and 5 the synthesis of bAuNPs was very low, however, pH 5 demonstrated a concentration increase as time progressed [GNP5.24.58 (0.17) to GNP5.72.58 (0.24)] (Table 3.1).

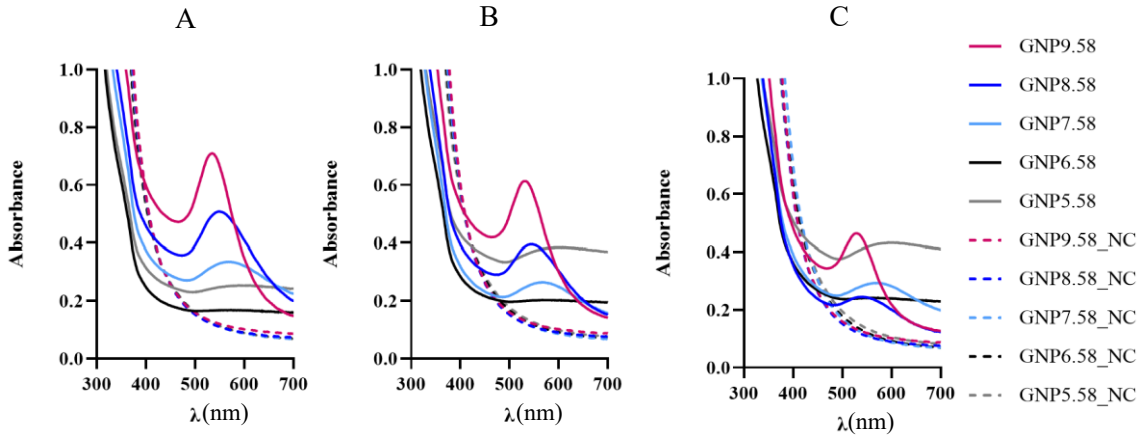

Figure 3.7 – UV-Vis spectra obtained for bAuNPs synthesized at 58 ºC for 24 h (A), 48 h (B) and 72 h (C) at different pH and the respective negative control (NC);

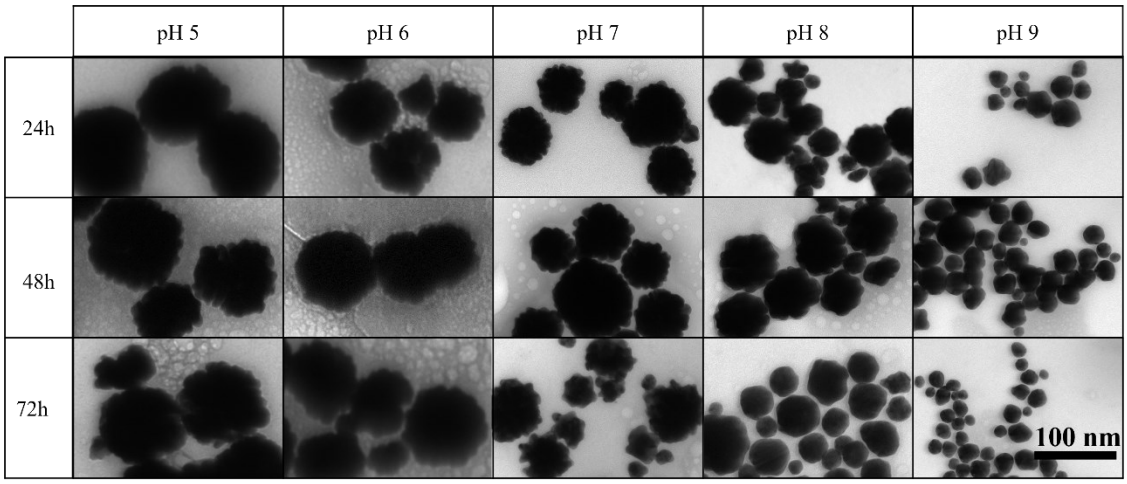

Figure 3.8 - TEM photographs of each bAuNP synthetized at 58 ºC at different pH and times (100 nm ampliation).

3.1.3.3 Effect of temperature in bAuNP synthesis

To understand the effect of temperature, AuNPs were synthetized at 29 ºC, 37 ºC, 50 ºC and 58 ºC. At lower temperatures the UV-Vis spectra showed low intensity peaks, what was translated in high aggregation and low concentration values (Table 3.1). As temperature increases, pH 9.0 and pH 8.0 showed surprising high intensity peaks (Fig. 3.9) accompanied by low aggregation values mainly at 50ºC [GNP9.24.50 (0.34) and GNP8.24.50 (0.49)] and 58ºC [GNP9.24.58 (0.23) and GNP8.24.58 (0.44)] (Table 3.1). Regarding concentration values, pH 9.0 showed a slight decrease at 58 ºC [GNP9.24.58 (0.38 mM)] and an even more pronounced decrease at pH 8.0 [GNP8.24.58 (0.30 mM)], in relation to the values obtained at 50 ºC [GNP9.24.50 (0.39 mM) and GNP8.24.50 (0.36 mM)] (Table 3.1). Looking for UV-Vis spectra, 37 ºC seems to be an optimal temperature for the synthesis of AuNPs at neutral pH 7.0 in terms of product yield [GNP7.24.37 (0.26 mM)] (Fig. 3.9A and Table 3.1), decreasing concentration [GNP7.24.50 (0.24 mM) and GNP7.24.58 (0.22 mM)] and aggregation [GNP7.24.50 (0.80) and GNP7.24.58 (0.72)] values as temperature is increased (Table 3.1). Contrarily, for pH 5 and 6 higher aggregation values were obtained at higher temperatures [GNP5.24.58 (1.00) and GNP6.24.58 (1.01)] (Table 3.1). UV-Vis spectra exhibited low intensity peaks, however, an intensity increase was noted for pH 6.0 and pH 5.0 at 50 ºC (GNP6.24.50) and at 58 ºC (GNP5.24.58) (Fig. 3.9).

In general, TEM analysis showed a slight decrease in size as temperature was raised (Table 3.1), with the particles maintaining raspberry or irregular shape (Fig. 3.10). The only

exception was the bAuNPs synthetized at pH 9.0 and pH 8.0 at 58 ºC [GNP9.24.58 and GNP8.24.58], presenting bAuNPs with cleaner and more rounded surface (more similar appearance to spherical nanostructures) (Fig. 3.10).

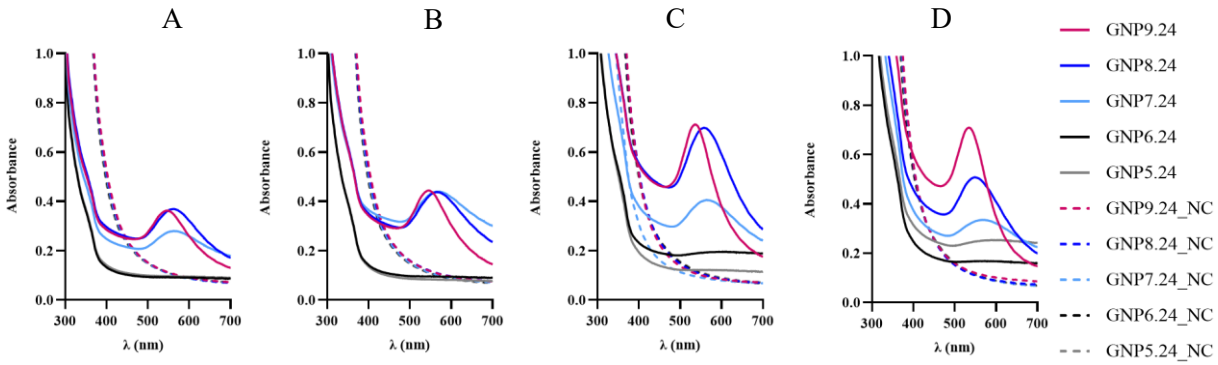

Figure 3.9 - UV-Vis spectrum obtained for bAuNPs synthesized at 29 ºC (A), 37 ºC (B), 50 ºC (C) and 58 ºC (D) for 24 h at different pH and the respective negative control (NC).

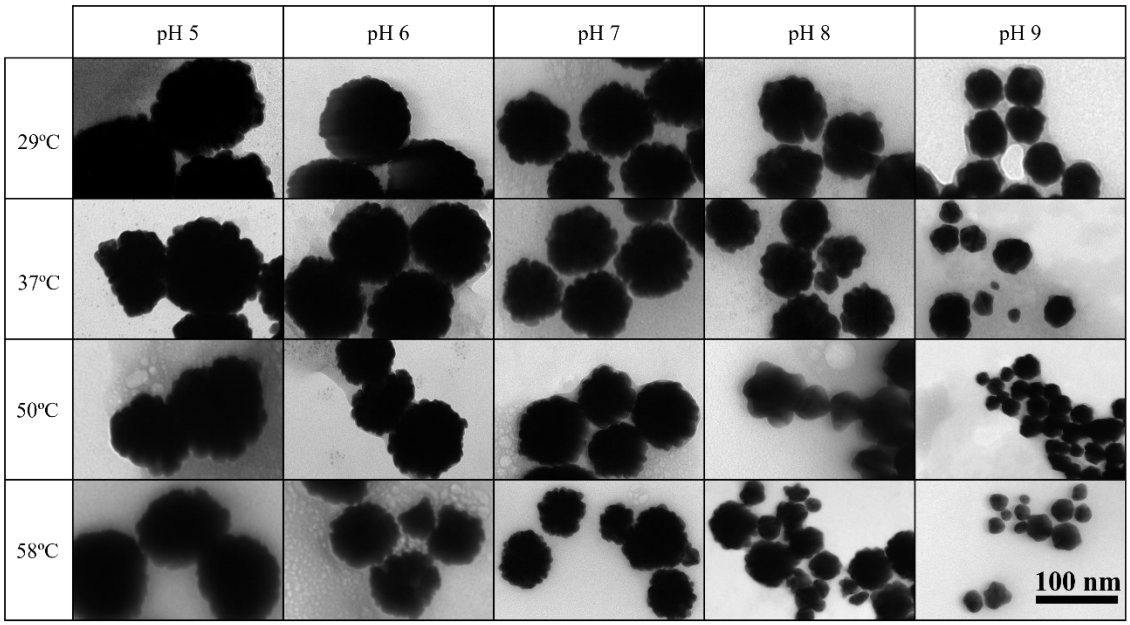

Figure 3.10 - TEM photographs of each bAuNP synthetized for 24 h at different pH and temperature (100 nm ampliation).

3.1.3.4 Attenuated Total Reflection Fourier-Transform Infrared Spectroscopy - ATR-FT-IR

The normalized ATR-FT-IR spectra of the gold nanoparticles GNP9.24.50, GNP9.24.58 and GNP8.24.50 are depicted in Fig. 3.11.

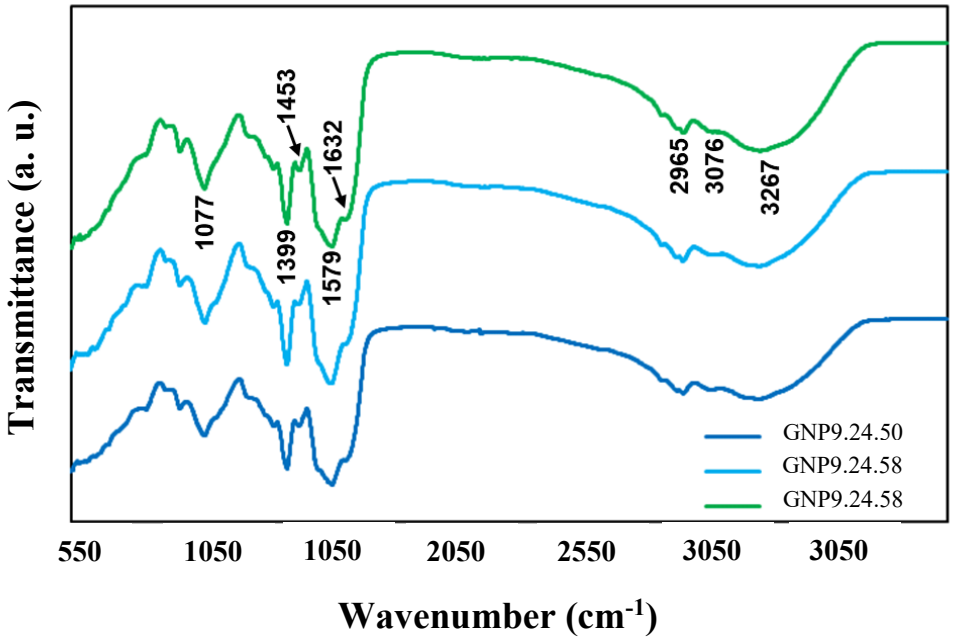

Figure 3.11 - ATR-FT-IR spectra of the gold nanoparticles GNP9.24.50, GNP9.24.58, and GNP8.24.50.

The analysis of the spectra highlighted in Fig. 3.11 allows inferring that the three products exhibit similar spectral properties. All spectra exhibit a strong and broad vibration band at 3267 cm^{-1} that can be assigned to the stretching of the hydroxyl groups; a weak vibration at 3076 cm^{-1} characteristic of the N-H stretching, and an absorption peak at *ca.* 2965 cm^{-1}, which can be attributed to the C-H stretching vibration of alkanes. All ATR-FT-IR spectra also exhibit vibrations at 1632 and 1579 cm^{-1} that can be assigned to amides containing carbonyl groups (C=O), and absorption bands at 1453, 1399 and 1077 cm^{-1} cm^{-1} that can be attributed to the C-O stretching vibrations of aromatic and aliphatic amines, respectively.

3.2 Cytotoxic effect evaluation of bAuNPs in prostate cell lines

The results of the prelaminar screening of the bAuNPs activity on prostate cell carcinoma are presented in the following subsections of this work. GNP9.24.58 at 10^{-3} mM showed a significant reduction of the viability, and a decreasing tendency in the proliferation of PC3 cells, not showing significant activity in HPEpiC cells. As a result, it was the only condition tested in the cellular uptake assay, the injury assay, and in the IL-6 ELISA assay.

3.2.1 bAuNPs cellular uptake assay

The representative photograph of the qualitative PC3 cell uptake assay shows red fluorescence, which indicates that bAuNPs (GNP9.24.58) adsorbed onto the cells (Fig. 3.12A). The blue color signifies the cell nucleus, which has been marked with DAPI (Fig. 3.12A). In contrast, the control photograph shows only the nucleus of the cells marked with DAPI, without any red fluorescence (Figure 3.12B). This indicates that in the absence of the bAuNPs, no adsorption onto the cells is observed.

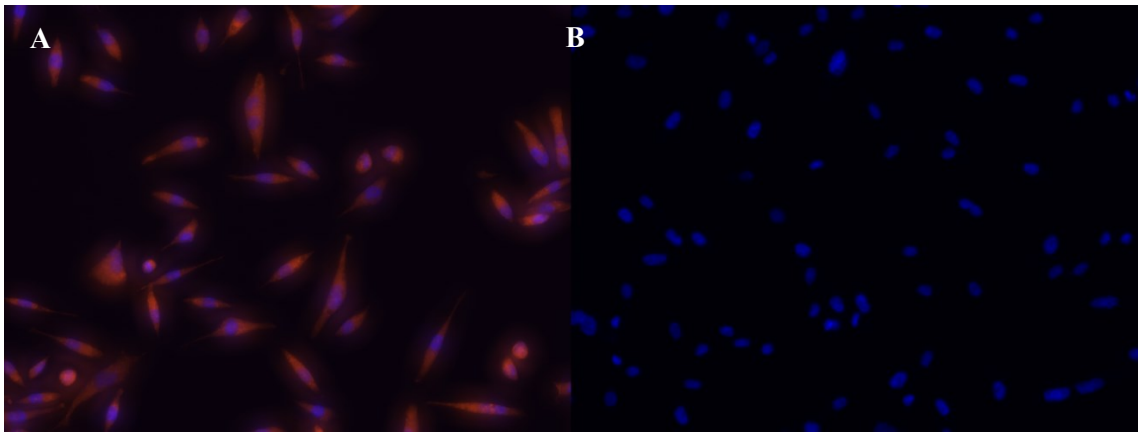

Figure 3.12 – (A) Representative microscope photograph of the qualitative PC3 cell uptake assay, in red is represented rhodamine B labelled bAuNPs dispersed on the cells and in blue the cell nucleus marked with DAPI; (B) Representative microscope photograph of the control (PC3 cells without addition of rhodamine B labelled bAuNPs), only the nuclei of the cells are marked with DAPI, and no fluorescence is capture in red.

3.2.2 Viability and Proliferation assay

The viability and proliferation assays were performed after 24 h of treatment with the bAuNPs (GNP9.24.50; GNP8.24.50 and GNP9.24.58). In all analyzed conditions, no dose-dependent relation was observed. Regarding the effect of AuNPs in HPEpiC cells, no

significant differences were found (Fig. 3.13), however, an increasing tendency in cell proliferation was noticed after treatment with GNP9.24.50 and GNP8.24.50 at 0.5-10^{-3} mM concentration range (Fig. 3.13B). For PC3 cells, only GNP9.24.58 at 10^{-3} mM has proved to have statistically significant ($p<0,05$) effect on cell viability (74%) (Fig. 3.13C), also showing a decreasing tendency on cell proliferation at the same concentration (Fig. 3.13D).

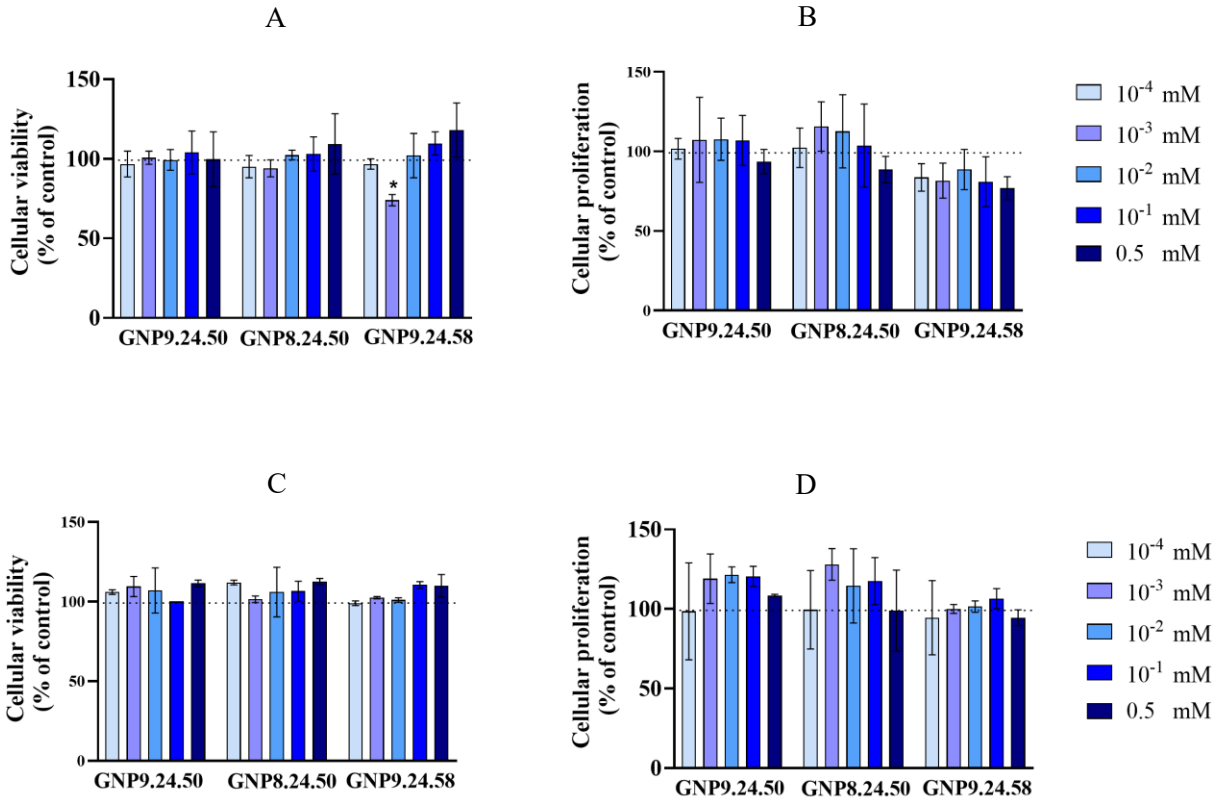

Figure 3.13 - Cellular viability (A) and proliferation (B) in percentage of control for **HPEpiC** cells after 24 h treatment with GNP9.24.50, GNP8.24.50 and GNP9.24.58 at different concentrations; Cellular viability (A) and proliferation (B) in percentage of control for **PC3 cells**, after 24 h treatment with GNP9.24.50, GNP8.24.50 and GNP9.24.58 at different concentrations. Legend: 0.5 to 10^{-4} mM: 0.5 mM to 0.0001 mM AuNPs; NC (0 mM): Negative control, without AuNPs.

3.2.3 Injury

The results of the injury assay are depicted in Fig. 3.14. The GNP9.24.58 (10^{-3} mM) did not produce any effect on the migration of HPEpiC cells after 24 h treatment (Fig. 3.14A), showing a complete wound closure (Fig. 3.14C). Contrarily, when the same bAuNP was applied in PC3 cells, at the same concentration, a prevention of wound closure was observed (Fig. 3.14F). In PC3 cells, cellular migration was significantly lower ($p<0,01$) in relation to control (75%) (Fig. 3.14D).

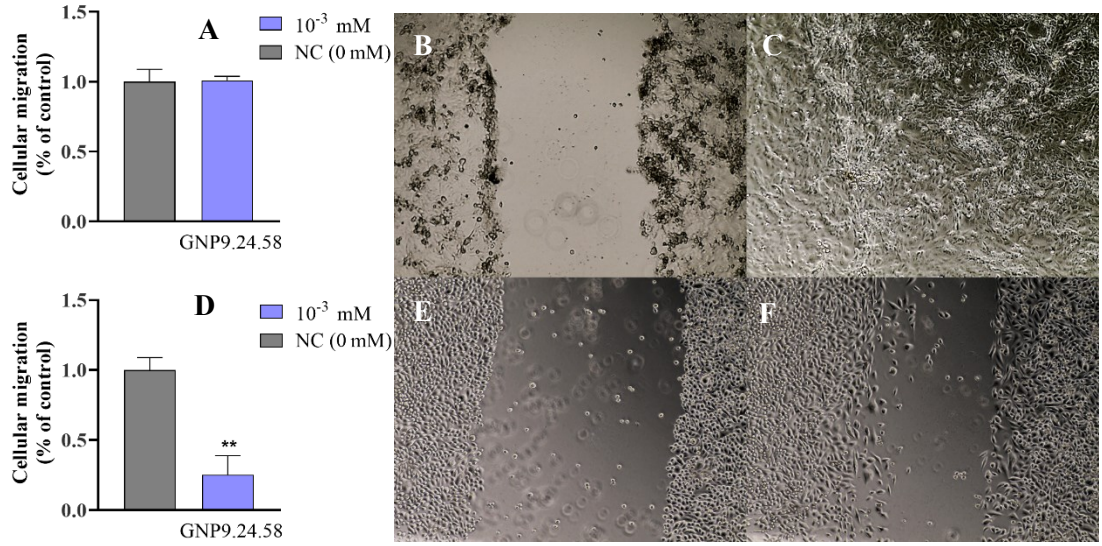

Figure 3.14 - Cellular migration of **HPEpiC cells** as percentage of control (A) after 24 h of treatment with GNP9.24.58 (10^{-3} mM) (blue bar) and after 24 h of growth without bAuNPs (NC, grey bars); Microscope photographs denoting the difference between 0 (B) and 24 h (C) of treatment with GNP9.24.58 (10^{-3} mM) of the **HPEpiC cells**; Cellular migration of **PC3 cells** in relation with the control (D) after 24 h of treatment with GNP9.24.58 at (10^{-3} mM) and after 24 h of growth without bAuNPs (NC, grey bars); Microscope photographs denoting the difference between 0 (E) and 24 h (F) of treatment with GNP9.24.58 at (10^{-3} mM) of **PC3 cells**. Legend: 10^{-3} mM: 0.001 mM AuNPs; NC (0 mM): Negative control, without AuNPs.

3.2.4 Human interleukin 6 (IL-6) ELISA assay

As shown in Fig. 3.4, GNP9.24.58 (10^{-3} mM) did not produce any effect on IL-6 levels of HPEpiC cells after 24 h of treatment (Fig. 3.15A). Contrarily, statistically significant ($p<0,05$) reduction (20%) was observed for PC3 cells (Fig.3.15B).

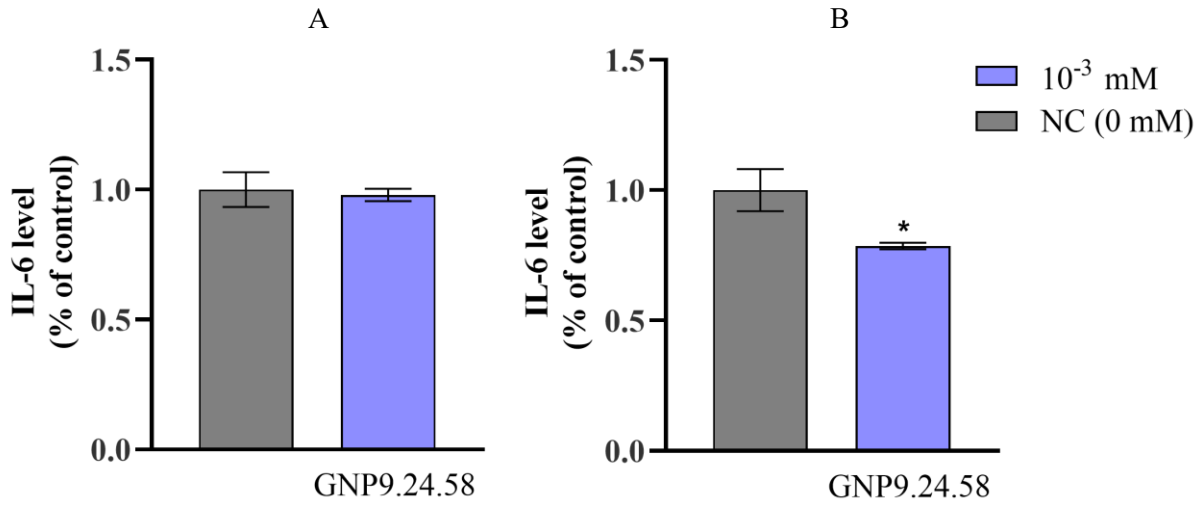

Figure 3.15 - IL-6 levels of HPEpiC cells (A) and PC3 cells (B) as percentage of control after 24 h of treatment with GNP9.24.58 at (10^{-3} mM) (blue bars) and after 24 h of growth without bAuNPs (NC, grey bars). Legend: 10^{-3} mM: 0.001 mM AuNPs; NC (0 mM): Negative control, without AuNPs.

3.3 AuNPs against Gram-negative and Gram-positive bacteria

The results of the prelaminar screening of the bAuNPs activity on the growth (kinetics) and viability of bacteria are described in the following subsections. GNP9.24.58 at 10^{-1} mM showed to reduce the growth all bacteria tested in 50% in relation to the control. As a result, it was the only condition tested in the viability assays. *E. coli* was found to be the most susceptible bacterium to this condition. The effect of this condition on MRSA and MSSA was similar, with both strains showing susceptibility. However, because MRSA is a resistant strain, it was considered more relevant to investigate the effect of GNP9.24.58 at 10^{-1} mM on its viability. Thus, E. coli and MRSA were the two bacteria tested in the viability assay.

3.3.1 AuNPs effect on bacterial growth – Kinetics

The effect of AuNPs on the bacteria total growth was evident for certain conditions in some of the bacterial species tested. A notorious effect was observed for GNP9.24.58 for all bacteria strains tested for the concentration of 10^{-1} mM. In comparison to the negative control, this bAuNP condition was able to suppress bacteria growth by 50% (Fig. 3.16). The GNP9.24.58 (10^{-1} mM) showed higher effect in Gram-negative bacteria, including, *E. coli* (30,97%) (Fig. 16A and B) and *K. pneumoniae* (46,20%) (Fig. 3.16C and D). In Gram-positive bacteria the effect was evident for MSSA (46,64%) (Fig. 3.16E and F) and MRSA (46,63%) (Fig.3.16G and H). Other AuNPs have showed less significant effect. For example, GNP9.24.50 presented relative total growth values under 60% in *E. coli* [58,58% (0,5mM)] (Appendix 2) and GNP8.24.50 showed relative growth values under 70% in MSSA [69,54% (0,5 mM)] (appendix 3) and *E. coli* [67,19% (0,5 mM)] (Appendix 2). Some nanoparticles showed to cause excessive growth (above the negative control curve) in the first hours of culture growth, followed by a marked decay (under the negative control curve). This effect was observed for example in *K. pneumoniae* [GNP9.24.50 (0,5mM)] (Appendix 2) and MRSA [GNP9.24.50 (0,5 mM) and GNP8.24.50 (0,5 mM)] (Appendix 3).

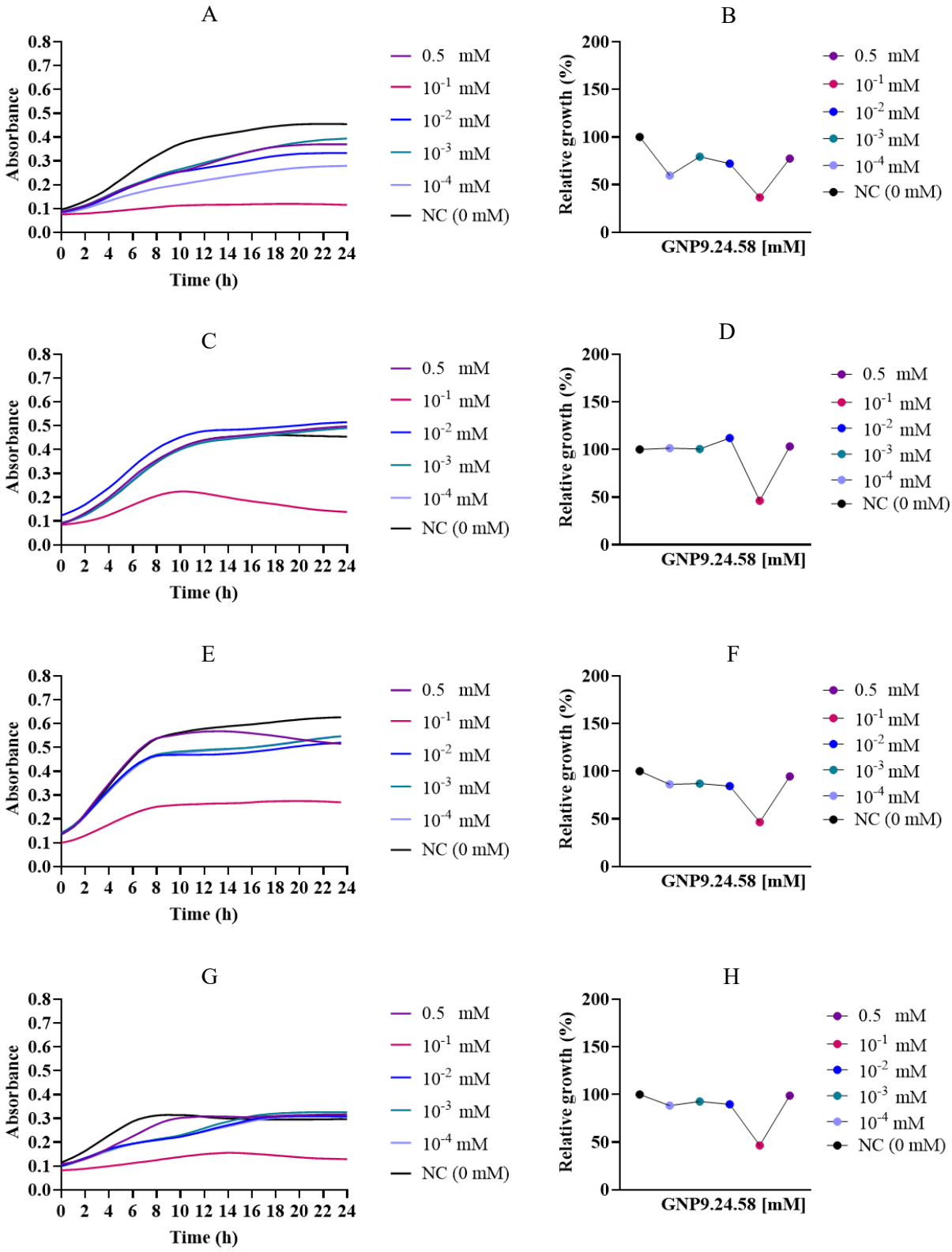

Figure 3.16 - Growth curves (A) and relative growth (B) of *E. coli* after 24 h of treatment with GNP9.24.58 at different concentrations; Growth curves (C) and relative growth (D) of *K. pneumoniae* after 24 h of treatment with GNP9.24.58 at different concentrations; Growth curves (E) and relative growth (F) of *MRSA* after 24 h of treatment with GNP9.24.58 at different concentrations; Growth curves (G) and relative growth (H) of *MSSA* after 24 h of treatment with GNP9.24.58 at different concentrations. Legend: 0.5 to 10^{-4} mM: 0.5 mM to 0.0001 mM AuNPs; NC (0 mM): Negative control, without AuNPs.

3.3.2 AuNPs effect on the viability of *E. coli* and MRSA

After 24 h of culture growth a significative reduction of the colony forming units (CFU) was observed (Table 4.1 and Fig. 3.17). GNP9.24.58 showed a higher capacity of reducing the viability in *E. coli* than in MRSA, presenting a significant statistical difference of 46,34% (Fig. 3.17A) and 59,66% (Fig.3.17B), respectively ($p<0,05$).

Table 4.1 – CFU/ml of *E. coli* and MRSA after 24 h of treatment with GNP9.24.58 (10^{-1} mM). Legend: 10^{-1} mM: 0.1 mM AuNPs; NC (0 mM): Negative control, without AuNPs.

	[AuNP] (mM)	CFU/ml
E. coli	NC	3,08E+08
	10^{-1}	1,43E+08
MRSA	NC	4,40E+08
	10^{-1}	2,63E+08

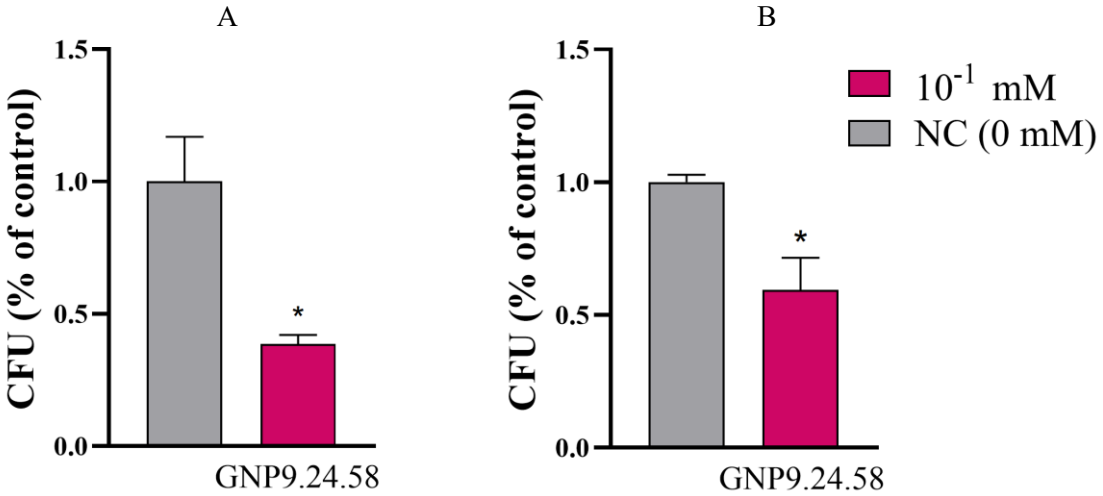

Figure 3.17 - CFU/ml of *E.coli* (A) and MRSA (B) as percentage of control after 24 h of treatment with GNP9.24.58 (10^{-1} mM). Legend: 10^{-1} mM: 0.1 mM AuNPs; NC (0 mM): Negative control, without AuNPs.

The following Fig. 3.18 is an example image of the results obtained during CFU counting and shows the cultures of *E. coli* and MRSA with and without the addition of bAuNPs.

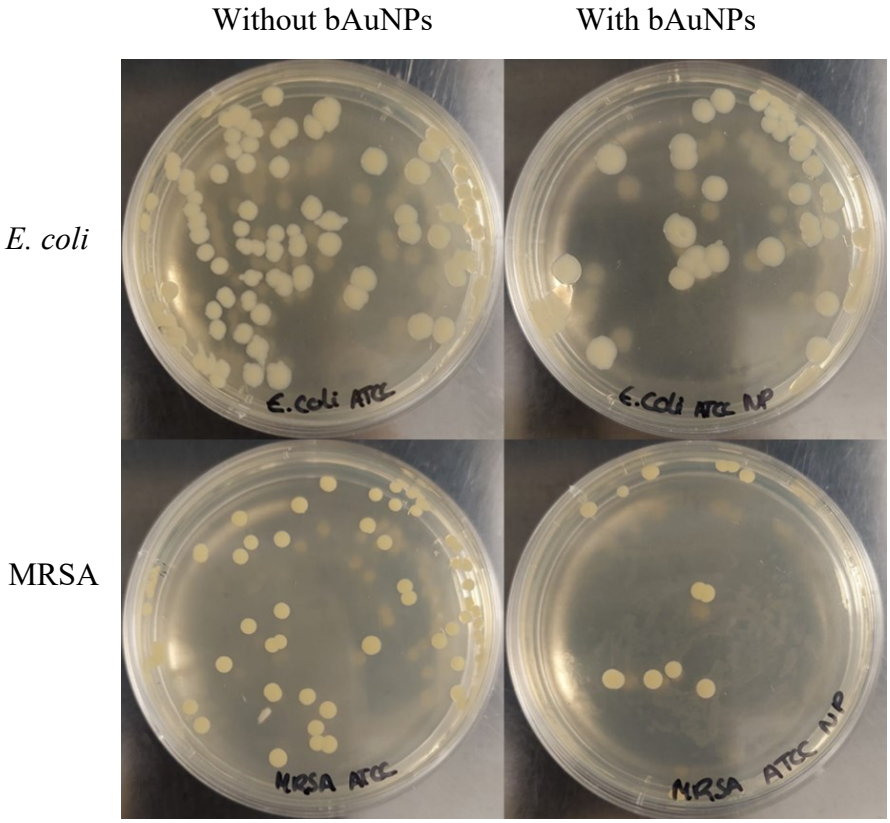

Figure 3.18 - Example image of *E. coli* (top images) and MRSA (bottom images) cultures at 10^{-7} dillution with (right) and without (left) bAuNPs.

4. Discussion

The metabolites present in *P. aeruginosa* have proven to be able to alter DCIP form its oxidized to its reduced form. When the bacterium was grown at an optical density 1.0 (OD_{600}) it was noticed that at 9h, the collected supernatant presented an increased potential for the reduction of this compound, leading to a surprising absorbance decay. After 15 h of bacterial growth, the supernatant appears to lose its reducing power, preventing the decay of DCIP absorbance, most likely due to fewer reducing species present in the supernatant at that specific time of bacterial growth. An intriguing fact is that the higher reducing potential appears to correspond with the late-exponential phase of bacterial growth, theoretically, in the phase where the production of secondary metabolites is higher (89). Based on the hypothesis presented by Nangia et al. which presents a putative mechanism for the biosynthesis of bAuNPs with the involvement of a NADPH-dependent enzyme (37) and knowing that DCIP can be directly reduced by NADPH, the greater decay of absorbance acquired at optical density 1.0 (OD_{600}) and at 9 h growth time may indicate the possibility of the same enzyme being involved in the mechanism of synthesis of bAuNPs by PAO1. This fact is corroborated by the subsequent synthesis of bAuNPs that was carried out with the extract of the bacterium after 0, 9 and 19 h of culture growth; the extract collected at 9 h proved capable of producing higher yields of bAuNPs, as would have been indicated by the DCIP results. This allowed us to define DCIP as a possible indicator of the culture conditions with the highest reducing potential. The condition defined at this point was then used for the following experiments. When the PAO1 mutant was used for the biosynthesis of AuNPs, the absence of the GR gene resulted in a lower yield of bAuNPs and in a lower absorbance decay after DCIP was added to the bacterium extract. These results allowed not only to reinforce the role of DCIP as an indicator of the reducing potential, but also to extrapolate the possible involvement of the GSH reductase in the biosynthesis of bAuNPs. However, the fact that the biosynthesis of bAuNPs has not been completely inhibited suggests the possibility that this process does not follow a single path.

With optimized culture conditions, the biosynthesis of the nanoparticles at different pH, time and temperature was conducted. It was verified that pH is one of the parameters with greatest influence on the synthesis of bAuNPs, especially in terms of their size, shape, and yield of the reaction. It was noticed that the size of the nanoparticles decreases with the increase in pH and that, conversely, the reaction yield increases. Among all parameters, pH seems to play a major role in the reducing power of secondary metabolites and enzymes present in the supernatant of bacterium (90). At high pH the OH^- ions present in the extract replace those of

Cl^- present in the $AuCl_4^-$ preventing the possible posterior growth of the nuclei by the repulsions between negatively charged ions of cell extract and gold ions, keeping the particles as small spheres (91). As observed by Sneha et al. and Armendáriz et al. lower pH originates particles with larger dimensions, which can be explained by an uncontrolled nucleation of particles resulting from the decrease of repulsions between $AuCl_4^-$ and the carboxylic groups present in the culture extract (92, 93). The reaction time does not seem to produce significant effects on the synthesis of bAuNPs; however, it is to notice that, at the lowest pH's tested (pH 5.0 and pH6), there was an increase in yield up to the 72 h time-point while, at higher pH's (pH 8.0 and pH 9.0) the yield decreases with the evolution of time. A hypothesis that could explain these findings is that because secondary metabolites and enzymes present in bacteria have less reducing power at lower pH, nucleation occurs more slowly and continues to occur over time. Supporting this theory is the growth of the crystal, where, for lower pH's, it seems to slowly increase with time, while for higher pH's there is a break of this trend at 48 h with a decrease in particle size. Following the same line of thinking, at higher pH, as there is greater availability of enzymes and metabolites, nucleation happens earlier, reaching the synthesis limit also faster. At 72h of incubation period, at pH 8.0 and 9.0, the instability of the particles was notorious with a reduction in the concentration and size of the nanoparticles, suggesting a decomposition phenomenon (94). The temperature also seems to influence both size and concentration of synthesized bAuNPs. For pH 7.0, 8.0 and 9.0 the temperature of 50ºC seems to be ideal, presenting the best synthesis yields. However, there seems to be an increase in instability accompanied again by the decomposition of particles when the temperature rises to 58ºC. At pH 5.0 and 6.0, the trend is an increase in bAuNPs concentration with increasing temperature, indicating that, despite obtaining lower concentrations than at higher pH, nanoparticles maintain better stability when the temperature is increased.

ATR-FT-IR results showed the presence of various compounds and could confirm the involvement of organic molecules in the bAuNPs synthesis process. The presence of C-O, probably due to amino acid residues may indicates that proteins from PAO1 extract co-exists with bAuNPs. This fact leads to the hypothesis that these co-existing proteins could be one of the factors influencing the rate of internalization of bAuNPs in tumor and bacteria cells. This could reduce the probability of cells to recognize bAuNPs as foreign agents internalizing them as a food supplement.

Taking the results described above, the conditions showing the most promising features for application as antitumor and antimicrobial agents were chosen. For these assays, the most

important parameter considered was concentration, aiming to opt for the condition with higher yield, envisioning greater economic profitability. Thus, the bAuNPs chosen were those synthesized at pH 9.0 for 24 h at 50 and 58 ºC (GNP9.24.50 and GNP9.24.58). However, to allow a better perception on the influence of the different characteristics resulting from different synthesis parameters in the activity against PCa and bacteria, bAuNPs synthetized at pH 8.0 for 24 h at 50 ºC (GNP8.24.50) were also tested.

In general, bAuNPs had little effect on cancer cells, at least in terms of cell viability and proliferation. Furthermore, there was no consistent increase in antitumoral potency with increasing concentration of bAuNPs, indicating that their effect may be dependent on their specific interactions with cells.

The presence of fluorescent red dots in the rodamine-B assay allowed the observation of bAuNP adherence to PC3 cells. Although this observation does not prove that the bAuNPs have been internalized, it does indicate that they are interacting with the cell membrane. Moreover, these results were also relevant from a functional point of view of bAuNPs. Since that, for the coating with rhodamine-B, there must be amine groups on the surface of the bAuNPs, the fluorescence observed supports the results obtained by AT-FT-IR, reinforcing the possible presence of amine groups co-existing with the bAuNPs.

In this study, it was possible to verify that among the three types of nanoparticles tested, GNP9.24.58 was the one that produced a higher anti-viability and anti-proliferation effect in PC3 cells without affecting HPEpiC cell. These results are in line with observations from other studies, which attribute greater potential to more spherical and smaller nanoparticles (48, 49). It was observed that, at 10^{-3} mM there was a statistically significant viability decrease ($p<0.05$) in PC3 cells. Although the same statistical significance was not noted for cell proliferation, there has been a downward trend in relation to the control line in this same concentration, indicating that, possibly, although viability is significantly reduced, there may not be a total cell death, allowing cells that remain alive to continue proliferating. However, after injury, there was a reduction in the migratory capacity in about 75%, compared to control. This fact became, from a clinical point of view, more preponderant. Nair et al. found that patient survival is significantly more strongly associated with predicted tumor migration levels than with predicted tumor proliferation levels (95). As a complement, IL-6 levels on PC3 and HPEpiC cultures were also quantified. Although IL-6 is an important protein in the regulation of the inflammatory process, it can't be assumed that a decrease in IL-6 levels, after treatment with AuNPs, directly results in a reduction of the tumor aggressiveness. As such, it is necessary to

take into account that IL-6 belongs to a complex regulatory mechanism of the inflammatory response that involves other key players. Regardless, this protein has been associated with tumor growth at specific stages of tumor progression. Considering the results obtained (Fig. 3.15B), it is possible to verify that the levels of IL-6 presented a decreasing tendency, as observed by Al-Trad B. et al. in their study about the effect of AuNPs against induced benign prostate carcinoma in rats (46), while, in HPEpiC cells, the levels were maintained. Nevertheless, further studies are needed to fully understand the mechanisms behind the observed potential of bAuNPs to downregulate inflammation in PC3 cells.

Considering the results for the antimicrobial assays, the effect of bAuNPs was higher in Gram-negative bacteria than in Gram-positive bacteria. Ahmad et al. and Kim et al. have obtained similar results in *E. coli* and *S. aureus* and attribute these results to the cell wall of *S. aureus* (a Gram-positive bacterium), which is much thicker than *E. coli* (a Gram-negative bacterium). The thinner peptidoglycan layer of *E. coli* may create less resistance to the bAuNPs, making it more susceptible compared to *S. aureus* (83, 96). Morones et al. and Alahmadi et al. also relate the greater effect of the nanoparticles with the smaller size and greater contact area of these structures, which is reported to produce electronic effects, which are defined as changes in the surface's local electronic structure as a result of size, increasing the reactivity of NPs surface (97, 98). These observations agree with the results obtained in the present work, where GNP9.24.58 (10^{-1} mM) was the condition that prompted the smallest and most spherical bAuNP, and the one that produced the greatest bactericidal effects.

In MRSA, GNP9.24.50 (0.5 mM) and GNP8.24.50 (0.5 mM) have proved to produce an excessive growth in the first hours of culture, followed by a marked growth decay. This effect was also noted for *K. pneumoniae* after treatment with GNP9.24.50 (0.5 mM).

When bacteria are exposed to stressors such as antimicrobials or NPs, they can undergo a process called adaptive stress response, which involves the activation of specific metabolic pathways in order to adapt to the new conditions (99). These pathways can involve the production of protective molecules or the activation of repair mechanisms, which can allow the bacteria to survive and continue growing under stressful conditions (100). One of the hypotheses for the aforementioned results, is that bAuNPs initially induced an adaptive stress response, leading to an initial increase in growth. However, as bacteria continued to grow and consume resources, the metabolic demands of this response may have become unsustainable, leading to a decrease in growth (101). Other possible explanation is that the adaptative stress

response caused by bAuNPs, lead to a faster consumption of the surrounding medium, leading to its faster depletion, resulting in a growth decrease (102).

The effect of bAuNPs observed in PCa cells regarding a non-regular dose-response effect was also observed in the bacteria assays, where increased concentration of bAuNPs, did not necessarily correlate with an increased antimicrobial effect. Although these findings conflict with the results obtained by Ahmad et al. and Folorunso et al. (83, 84), they help to reinforce the assumption that the effect of AuNPs is not linearly related to increasing concentration. This fact increases the importance of choosing an ideal concentration. Further research is needed to fully understand the mechanisms behind the bactericidal activity of AuNPs and to optimize their use as antimicrobial agents. Given the increasing prevalence of antibiotic resistance and the need for alternative antimicrobial agents, the development of AuNPs as a potential treatment option is a promising area of research (64).

Choosing the appropriate concentration can be relevant when considering AuNPs in a therapeutic context. In long run, this could be translated into more efficient therapeutic methods that are also more cost-effective, since lower doses can provide better treatment outcome. Parallelly, the risk of using a higher concentration that no longer has the intended effect, and can even potentiate adverse effects, is reduced.

5. Conclusion

P. aeruginosa extracts proved to be capable of synthesizing gold nanoparticles. Additionally, it was possible to establish DCIP as a possible method of screening the most favorable culture conditions aimed at obtaining the best yields in the biosynthesis of bAuNPs. Thus, comparing the yield at three different culture times, it was observed that PAO1 cultures at 9h of growth and at 37ºC allow obtaining extracts that potentiate the bAuNPS synthesis. This method allowed also to observe that the lack of GR gene in PAO1 resulted in a minor reducing potential, decreasing the synthesis yields of bAuNPs.

Among the physico-chemical parameters tested, pH seems to be the one that exerts the greatest influence on the synthesis of bAuNPs, along with temperature. Among all the conditions tested, bAuNPs synthesized at pH 9.0 for 24 h at 58 ºC (GNP9.24.58) showed the highest synthesis yields and more spherical, smaller, and less aggregated nanoparticles. Furthermore, ATR-FT-IR results revealed characteristic absorption bands of amines, most likely due to proteins co-existing with bAuNPs, which may reduce cell recognition of bAuNPs as foreign agents and increase their internalization as a food supplement.

Considering AuNPs potential against tumor cells, a significant reduction in viability and a decreasing tendency in proliferation was observed for GNP9.24.58 at 10^{-3} mM, without affecting significatively HPEpiC cells. Additionally, this bAuNP condition has also demonstrated great capacity to prevent migration and some potential to decrease IL-6 levels of PC3 cells, not affecting HPEpiC cells in a significant way.

Regarding AuNPs potential against bacteria, it was noticed that GNP9.24.58 (10^{-1} mM) was the only condition capable of reducing by 50% the total growth of the Gram-negative and Gram-positive bacteria tested. Furthermore, the viability assays showed greater bactericidal potential of this condition in *E. coli* in relation to its potential in MRSA.

Interestingly, a close relation between the effect of bAuNPs in cancer cells and in bacteria cells was noticed. In a firsthand, no dose dependent effect with increasing bAuNPs concentration was observed for the two applications. Furthermore, the smaller and more spherical bAuNP (GNP9.24,58) proved to be more successful against both cancer cells and bacterial cells, which could suggest a similar mechanism of action.

Thus, along with the benefits of using PAO1 to produce nanoparticles: the process simplicity, the good yields and biocompatibility obtained; the control of shape, size, and

aggregation, also could be used to improve the therapeutic approaches to PCa and bacteria, contributing for targeted, cheaper, and greener therapies.

6. Future Perspectives

Although the present work has given some insights on how to potentiate *P. aeruginosa* to produce nanoparticles, it has allowed, among those tested, to verify which are the most important parameters for its synthesis and which of the nanoparticles obtained have the best potential against bacteria and prostate cancer, further studies are needed.

First, taking into account the increase in concentration, sphericity and decrease in size with increasing pH the next step will be to test higher pH and characterize the bAuNPs again. Regarding characterizations, in order to validate the crystalline structure of bAuNPs, supplementary methods to ATR-FT-IR must be used (e.g. Single-Crystal X-Ray Diffraction). Then, it is also necessary to apply inductively coupled plasma mass spectroscopy (ICP-MS) analyses, to be able to confirm the internalization of nanoparticles in both tumoral and bacterial cells. After this confirmation, a coating will be performed with aptamers specifically designed to bind to specific receptors for both bacteria and for PCa of the "naked" bAuNPs that proved to have a greater bactericidal and antitumor activity. After success in this specific recognition, a radiofrequency hyperthermia approach will be used, aiming to increase the effect of nanoparticles for both tumor and bacterial cells.

Lately, it is intended to test the bAuNPs coated with aptamers in live animal models with induced prostatic tumorigenesis and inoculated with pathogenic and resistant bacteria. Administering the nanoparticles in a vaccine format and using radiofrequency hyperthermia as a co-adjuvant therapy.

7. Bibliography

1. Singh H, Du J, Singh P, Mavlonov GT, Yi TH. Development of superparamagnetic iron oxide nanoparticles via direct conjugation with ginsenosides and its in-vitro study. J Photochem Photobiol B. 2018;185:100-10.
2. Schrofel A, Kratosova G, Safarik I, Safarikova M, Raska I, Shor LM. Applications of biosynthesized metallic nanoparticles - a review. Acta Biomater. 2014;10(10):4023-42.
3. Tao Y, Li M, Ren J, Qu X. Metal nanoclusters: novel probes for diagnostic and therapeutic applications. Chem Soc Rev. 2015;44(23):8636-63.
4. Nejati K, Dadashpour M, Gharibi T, Mellatyar H, Akbarzadeh A. Biomedical Applications of Functionalized Gold Nanoparticles: A Review. Journal of Cluster Science. 2021;33(1):1-16.
5. Gold Nanoparticles Market: Global Industry Trends, Share, Size, Growth, Opportunity and Forecast 2022-2027. IMARC Group; 2022. Report No.: 5615278.
6. Gold Nanoparticles Market - Growth, Trends, COVID-19 Impact, and Forecasts (2022 - 2027). Mordor Intelligence; 2022. Report No.: 4773686.
7. Gold Nanoparticles - Global Market Trajectory & Analytics. Global Industry Analysts, Inc; 2022. Report No.: 4805026.
8. Yeh YC, Creran B, Rotello VM. Gold nanoparticles: preparation, properties, and applications in bionanotechnology. Nanoscale. 2012;4(6):1871-80.
9. Liu J, Qin G, Raveendran P, Ikushima Y. Facile "green" synthesis, characterization, and catalytic function of beta-D-glucose-stabilized Au nanocrystals. Chemistry. 2006;12(8):2131-
10. Raveendran P, Fu J, Wallen SL. A simple and “green” method for the synthesis of Au, Ag, and Au–Ag alloy nanoparticles. Green Chem. 2006;8(1):34-8.
11. Ma Y, Kuang Q, Jiang Z, Xie Z, Huang R, Zheng L. Synthesis of trisoctahedral gold nanocrystals with exposed high-index facets by a facile chemical method. Angew Chem Int Ed Engl. 2008;47(46):8901-4.
12. Ye Y, Lv M, Zhang X, Zhang Y. Colorimetric determination of copper(ii) ions using gold nanoparticles as a probe. RSC Advances. 2015;5(124):102311-7.
13. Su K-H, Wei Q-H, Zhang X, Mock JJ, Smith DR, Schultz S. Interparticle Coupling Effects on Plasmon Resonances of Nanogold Particles. Nano letters. 2003;3(8):1087–90.
14. Huang X, El-Sayed MA. Gold nanoparticles: Optical properties and implementations in cancer diagnosis and photothermal therapy. Journal of Advanced Research. 2010;1(1):13-28.

15. Liu XY, Wang JQ, Ashby CR, Jr., Zeng L, Fan YF, Chen ZS. Gold nanoparticles: synthesis, physiochemical properties and therapeutic applications in cancer. Drug Discov Today. 2021;26(5):1284-92.
16. Singh P, Pandit S, Mokkapati V, Garg A, Ravikumar V, Mijakovic I. Gold Nanoparticles in Diagnostics and Therapeutics for Human Cancer. Int J Mol Sci. 2018;19(7).
17. Lv W, Gu C, Zeng S, Han J, Jiang T, Zhou J. One-Pot Synthesis of Multi-Branch Gold Nanoparticles and Investigation of Their SERS Performance. Biosensors (Basel). 2018;8(4).
18. Jenkins JA, Wax TJ, Zhao J. Seed-Mediated Synthesis of Gold Nanoparticles of Controlled Sizes To Demonstrate the Impact of Size on Optical Properties. Journal of Chemical Education. 2017;94(8):1090-3.
19. Levy A, De Anda Villa M, Laurens G, Blanchet V, Bozek J, Gaudin J, et al. Surface Chemistry of Gold Nanoparticles Produced by Laser Ablation in Pure and Saline Water. Langmuir. 2021;37(19):5783-94.
20. Suarez-Lopez R, Puntes VF, Bastus NG, Herves C, Jaime C. Nucleation and growth of gold nanoparticles in the presence of different surfactants. A dissipative particle dynamics study. Sci Rep. 2022;12(1):13926.
21. Salem SS, Fouda A. Green Synthesis of Metallic Nanoparticles and Their Prospective Biotechnological Applications: an Overview. Biol Trace Elem Res. 2021;199(1):344-70.
22. Ahmed S, Annu, Ikram S, Yudha SS. Biosynthesis of gold nanoparticles: A green approach. J Photochem Photobiol B. 2016;161:141-53.
23. Srinath BS, Namratha K, Byrappa K. Eco-Friendly Synthesis of Gold Nanoparticles by Bacillus subtilis and Their Environmental Applications. Advanced Science Letters. 2018;24(8):5942-6.
24. Iqtedar M, Aslam M, Akhyar M, Shehzaad A, Abdullah R, Kaleem A. Extracellular biosynthesis, characterization, optimization of silver nanoparticles (AgNPs) using Bacillus mojavensis BTCB15 and its antimicrobial activity against multidrug resistant pathogens. Prep Biochem Biotechnol. 2019;49(2):136-42.
25. Prabhu S, Poulose EK. Silver nanoparticles: mechanism of antimicrobial action, synthesis, medical applications, and toxicity effects. International Nano Letters. 2012;2(32).
26. Makarov VV, Love AJ, Sinitsyna OV, Makarova SS, Yaminsky IV, Taliansky ME, et al. "Green" nanotechnologies: synthesis of metal nanoparticles using plants. Acta Naturae. 2014;6(1):35-44.

27. Li X, Robinson SM, Gupta A, Saha K, Jiang Z, Moyano DF, et al. Functional Gold Nanoparticles as Potent Antimicrobial Agents against Multi-Drug-Resistant Bacteria. ACS Nano. 2014;8(10): 10682–6.

28. Arai H. Regulation and Function of Versatile Aerobic and Anaerobic Respiratory Metabolism in Pseudomonas aeruginosa. Frontiers in Microbiology. 2011;2.

29. Zhang Z, Zhang X. Evolution of Subfamily I.1 Lipases in Pseudomonas aeruginosa. Curr Microbiol. 2021;78(9):3494-504.

30. Willcox MD. Pseudomonas aeruginosa infection and inflammation during contact lens wear: a review. Optom Vis Sci. 2007;84(4):273-8.

31. Harshita, Chanchal, Jain D. Cloning, expression, purification, crystallization and initial crystallographic analysis of FleN from Pseudomonas aeruginosa. Acta Crystallogr F Struct Biol Commun. 2016;72(Pt 2):135-8.

32. Azam MW, Khan AU. Updates on the pathogenicity status of Pseudomonas aeruginosa. Drug Discov Today. 2019;24(1):350-9.

33. Onbasli D, Aslim B. Determination of antimicrobial activity and production of some metabolites by Pseudomonas aeruginosa B1 and B2 in sugar beet molasses. African Journal of Biotechnology 2008;7(24).

34. Anayo OF, Scholastica EC, Peter OC, Nneji UG, Obinna A, Mistura LO. The Beneficial Roles of Pseudomonas in Medicine, Industries, and Environment: A Review. Pseudomonas aeruginosa - An Armory Within. 292019. p. 1522-32.

35. Abd El-Aziz M, Badr Y, Mahmoud MA. Biosynthesis of Gold Nanoparticles Using Pseudomonas Aeruginosa. AIP Conference Proceedings2007. p. 177-81.

36. Timoszyk A, Niedbach J, Śliżewska P, Mirończyk A, Kozioł JJ. Eco-Friendly and Temperature Dependent Biosynthesis of Gold Nanoparticles Using the Bacterium Pseudomonas aeruginosa: Characterization and Antibacterial Activity. Journal of Nano Research. 2017;48:114-24.

37. Nangia Y, Wangoo N, Goyal N, Shekhawat G, Suri CR. A novel bacterial isolate Stenotrophomonas maltophilia as living factory for synthesis of gold nanoparticles. Microbial Cell Factories. 2009;8(1).

38. Michie KL, Dees JL, Fleming D, Moustafa DA, Goldberg JB, Rumbaugh KP, et al. Role of Pseudomonas aeruginosa Glutathione Biosynthesis in Lung and Soft Tissue Infection. Infect Immun. 2020;88(6).

39. H. Kwon D, Abualnoor A. Glutathione Reductase Encoding Gene (gor) is Associated with Oxidative Stress and Antibiotic Susceptibility in Pseudomonas aeruginosa. Annual Research & Review in Biology. 2021:1-8.
40. GLOBOCAN. The Global Cancer Observatory - CANCER FACT SHEETS. World Health Organization 2020.
41. Chaturvedi VK, Singh A, Singh VK, Singh MP. Cancer Nanotechnology: A New Revolution for Cancer Diagnosis and Therapy. Curr Drug Metab. 2019;20(6):416-29.
42. Medici S, Peana M, Coradduzza D, Zoroddu MA. Gold nanoparticles and cancer: Detection, diagnosis and therapy. Semin Cancer Biol. 2021;76:27-37.
43. Sfanos KS, De Marzo AM. Prostate cancer and inflammation: the evidence. Histopathology. 2012;60(1):199-215.
44. Haverkamp J, Charbonneau B, Ratliff TL. Prostate inflammation and its potential impact on prostate cancer: a current review. J Cell Biochem. 2008;103(5):1344-53.
45. Gueron G, De Siervi A, Vazquez E. Advanced prostate cancer: reinforcing the strings between inflammation and the metastatic behavior. Prostate Cancer Prostatic Dis. 2012;15(3):213-21.
46. Al-Trad B, Aljabali A, Al Zoubi M, Shehab M, Omari S. Effect of gold nanoparticles treatment on the testosterone-induced benign prostatic hyperplasia in rats. Int J Nanomedicine. 2019;14:3145-54.
47. Slepicka P, Kasalkova NS, Siegel J, Kolska Z, Bacakova L, Svorcik V. Nano-structured and functionalized surfaces for cytocompatibility improvement and bactericidal action. Biotechnol Adv. 2015;33(6 Pt 2):1120-9.
48. Tarantola M, Pietuch A, Schneider D, Rother J, Sunnick E, Rosman C, et al. Toxicity of gold-nanoparticles: synergistic effects of shape and surface functionalization on micromotility of epithelial cells. Nanotoxicology. 2011;5(2):254-68.
49. Wozniak A, Malankowska A, Nowaczyk G, Grzeskowiak BF, Tusnio K, Slomski R, et al. Size and shape-dependent cytotoxicity profile of gold nanoparticles for biomedical applications. J Mater Sci Mater Med. 2017;28(6):92.
50. Steckiewicz KP, Barcinska E, Malankowska A, Zauszkiewicz-Pawlak A, Nowaczyk G, Zaleska-Medynska A, et al. Impact of gold nanoparticles shape on their cytotoxicity against human osteoblast and osteosarcoma in in vitro model. Evaluation of the safety of use and anti-cancer potential. J Mater Sci Mater Med. 2019;30(2):22.
51. Liu X, Wu F, Tian Y, Wu M, Zhou Q, Jiang S, et al. Size Dependent Cellular Uptake of Rod-like Bionanoparticles with Different Aspect Ratios. Sci Rep. 2016;6:24567.

52. Zhao F, Zhao Y, Liu Y, Chang X, Chen C, Zhao Y. Cellular uptake, intracellular trafficking, and cytotoxicity of nanomaterials. Small. 2011;7(10):1322-37.
53. Xie X, Liao J, Shao X, Li Q, Lin Y. The Effect of shape on Cellular Uptake of Gold Nanoparticles in the forms of Stars, Rods, and Triangles. Sci Rep. 2017;7(1):3827.
54. Bharadwaj KK, Rabha B, Pati S, Sarkar T, Choudhury BK, Barman A, et al. Green Synthesis of Gold Nanoparticles Using Plant Extracts as Beneficial Prospect for Cancer Theranostics. Molecules. 2021;26(21).
55. Hanan NA, Chiu HI, Ramachandran MR, Tung WH, Mohamad Zain NN, Yahaya N, et al. Cytotoxicity of Plant-Mediated Synthesis of Metallic Nanoparticles: A Systematic Review. Int J Mol Sci. 2018;19(6).
56. Fratoddi I, Venditti I, Cametti C, Russo MV. The puzzle of toxicity of gold nanoparticles. The case-study of HeLa cells. Toxicology Research. 2015;4(4):796-800.
57. Botha TL, Elemike EE, Horn S, Onwudiwe DC, Giesy JP, Wepener V. Cytotoxicity of Ag, Au and Ag-Au bimetallic nanoparticles prepared using golden rod (Solidago canadensis) plant extract. Sci Rep. 2019;9(1):4169.
58. Bodelón G, Costas C, Pérez-Juste J, Pastoriza-Santos I, Liz-Marzán LM. Gold nanoparticles for regulation of cell function and behavior. Nano Today. 2017;13:40-60.
59. Fratoddi I, Venditti I, Cametti C, Russo MV. How toxic are gold nanoparticles? The state-of-the-art. Nano Research. 2015;8(6):1771-99.
60. Prema P, Boobalan T, Arun A, Rameshkumar K, Babu RS, Veeramanikandan V, et al. Green tea extract mediated biogenic synthesis of gold nanoparticles with potent anti-proliferative effect against PC-3 human prostate cancer cells. Materials Letters. 2022;306(130893).
61. Nambiar S, Osei E, Fleck A, Darko J, Mutsaers AJ, Wettig S. Synthesis of curcumin-functionalized gold nanoparticles and cytotoxicity studies in human prostate cancer cell line. Applied Nanoscience (2018;8:347–57.
62. Allaker RP, Vargas-Reus MA, Ren GG. Nanometals as Antimicrobials. Antimicrobial Polymers2011. p. 327-50.
63. Organization WH. Antimicrobial resistance 2021 [Available from: https://www.who.int/news-room/fact-sheets/detail/antimicrobial-resistance.
64. Grace AN, Pandian K. Antibacterial efficacy of aminoglycosidic antibiotics protected gold nanoparticles—A brief study. Colloids and Surfaces A: Physicochemical and Engineering Aspects. 2972007. p. 63-70.

65. Pakbin B, Bruck WM, Rossen JWA. Virulence Factors of Enteric Pathogenic Escherichia coli: A Review. Int J Mol Sci. 2021;22(18).
66. Mylotte JM, Tayara A, Goodnough S. Epidemiology of bloodstream infection in nursing home residents: evaluation in a large cohort from multiple homes. Clin Infect Dis. 2002;35(12):1484-90.
67. McCue JD. Gram-negative bacillary bacteremia in the elderly: incidence, ecology, etiology, and mortality. J Am Geriatr Soc. 1987;35(3):213-8.
68. Jain S, Self WH, Wunderink RG, Fakhran S, Balk R, Bramley AM, et al. Community-Acquired Pneumonia Requiring Hospitalization among U.S. Adults. N Engl J Med. 2015;373(5):415-27.
69. Mueller M, Tainter CR. Escherichia Coli. StatPearls. Treasure Island (FL)2022.
70. Cui Y, Zhao Y, Tian Y, Zhang W, Lu X, Jiang X. The molecular mechanism of action of bactericidal gold nanoparticles on Escherichia coli. Biomaterials. 2012;33(7):2327-33.
71. Ronning TG, Aas CG, Stoen R, Bergh K, Afset JE, Holte MS, et al. Investigation of an outbreak caused by antibiotic-susceptible Klebsiella oxytoca in a neonatal intensive care unit in Norway. Acta Paediatr. 2019;108(1):76-82.
72. Tsereteli M, Sidamonidze K, Tsereteli D, Malania L, Vashakidze E. Epidemiology of Carbapenem-Resistant Klebsiella Pneumoniae in Intensive Care Units of Multiprofile Hospitals in Tbilisi, Georgia. Georgian Med News. 2018(280-281):164-8.
73. Ashurst JV, Dawson A. Klebsiella Pneumonia. StatPearls. Treasure Island (FL)2022.
74. Nirwati H, Sinanjung K, Fahrunissa F, Wijaya F, Napitupulu S, Hati VP, et al. Biofilm formation and antibiotic resistance of Klebsiella pneumoniae isolated from clinical samples in a tertiary care hospital, Klaten, Indonesia. BMC Proc. 2019;13(Suppl 11):20.
75. Khosravi M, Mirzaie A, Kashtali AB, Noorbazargan H. Antibacterial, anti-efflux, anti-biofilm, anti-slime (exopolysaccharide) production and urease inhibitory efficacies of novel synthesized gold nanoparticles coated Anthemis atropatana extract against multidrug- resistant Klebsiella pneumoniae strains. Arch Microbiol. 2020;202(8):2105-15.
76. Wertheim HF, Melles DC, Vos MC, van Leeuwen W, van Belkum A, Verbrugh HA, et al. The role of nasal carriage in Staphylococcus aureus infections. Lancet Infect Dis. 2005;5(12):751-62.
77. Becker K, Schaumburg F, Fegeler C, Friedrich AW, Kock R, Prevalence of Multiresistant Microorganisms PMMS. Staphylococcus aureus from the German general population is highly diverse. Int J Med Microbiol. 2017;307(1):21-7.

78. Zingg BM. Managing burns in children. An intraoperative nursing care plan. AORN J. 1991;54(3):568-75.
79. Sim BL, McBryde E, Street AC, Marshall C. Multiple site surveillance cultures as a predictor of methicillin-resistant Staphylococcus aureus infections. Infect Control Hosp Epidemiol. 2013;34(8):818-24.
80. Ito T, Katayama Y, Hiramatsu K. Cloning and nucleotide sequence determination of the entire mec DNA of pre-methicillin-resistant Staphylococcus aureus N315. Antimicrob Agents Chemother. 1999;43(6):1449-58.
81. Chambers HF, Deleo FR. Waves of resistance: Staphylococcus aureus in the antibiotic era. Nat Rev Microbiol. 2009;7(9):629-41.
82. Baker S, Satish S. Biosynthesis of gold nanoparticles by Pseudomonas veronii AS41G inhabiting Annona squamosa L. Spectrochim Acta A Mol Biomol Spectrosc. 2015;150:691-5.
83. Ahmad T, Wani IA, Manzoor N, Ahmed J, Asiri AM. Biosynthesis, structural characterization and antimicrobial activity of gold and silver nanoparticles. Colloids Surf B Biointerfaces. 2013;107:227-34.
84. Folorunso A, Akintelu S, Oyebamiji AK, Ajayi S, Abiola B, Abdusalam I, et al. Biosynthesis, characterization and antimicrobial activity of gold nanoparticles from leaf extracts of Annona muricata. Journal of Nanostructure in Chemistry. 2019;9:111-7.
85. Abdel-Raouf N, Mohammad N, Al-Enazi, Ibraheem IBM. Green biosynthesis of gold nanoparticles using Galaxaura elongata and characterization

of their antibacterial activity. Arabian Journal of Chemistry. 2013;10:3029-39.
86. Geethalakshmi R, Sarada DV. Gold and silver nanoparticles from Trianthema decandra: synthesis, characterization, and antimicrobial properties. Int J Nanomedicine. 2012;7:5375-84.
87. Dupuy C, Kaniewski J, Ohayon R, Deme D, Virion A, Pommier J. Nonenzymatic NADPH-dependent reduction of 2,6-dichlorophenol-indophenol. Anal Biochem. 1990;191(1):16-20.
88. Scarabelli L, Sanchez-Iglesias A, Perez-Juste J, Liz-Marzan LM. A "Tips and Tricks" Practical Guide to the Synthesis of Gold Nanorods. J Phys Chem Lett. 2015;6(21):4270-9.
89. Seyedsayamdost MR. Toward a global picture of bacterial secondary metabolism. J Ind Microbiol Biotechnol. 2019;46(3-4):301-11.
90. Das SK, Das AR, Guha AK. Microbial synthesis of multishaped gold nanostructures. Small. 2010;6(9):1012-21.

91. Kumari M, Mishra A, Pandey S, Singh SP, Chaudhry V, Mudiam MK, et al. Physico-Chemical Condition Optimization during Biosynthesis lead to development of Improved and Catalytically Efficient Gold Nano Particles. Sci Rep. 2016;6:27575.
92. Sneha K, Sathishkumar M, Kim S, Yun Y-S. Counter ions and temperature incorporated tailoring of biogenic gold nanoparticles. Process Biochemistry. 2010;45(9):1450-8.
93. Armendáriz V, Miguel JY, Duarte Moller A, Peralta Videa JRT, Horacio EstebanIcon, Herrera I, Gardea Torres JL. HRTEM characterization of gold nanoparticles produced by wheat biomass. Revista Mexicana de Física. 2004;50:7-11.
94. Zopes D, Stein B, Mathur S, Graf C. Improved stability of "naked" gold nanoparticles enabled by in situ coating with mono and multivalent thiol PEG ligands. Langmuir. 2013;29(36):11217-26.
95. Nair NU, Das A, Rogkoti VM, Fokkelman M, Marcotte R, de Jong CG, et al. Migration rather than proliferation transcriptomic signatures are strongly associated with breast cancer patient survival. Sci Rep. 2019;9(1):10989.
96. Kim J, Fiore AM, Lee H-H. Influences of online store perception, shopping enjoyment, and shopping involvement on consumer patronage behavior towards an online retailer. Journal of Retailing and Consumer Services. 2007;14(2):95-107.
97. Morones JR, Elechiguerra JL, Camacho A, Holt K, Kouri JB, Ramirez JT, et al. The bactericidal effect of silver nanoparticles. Nanotechnology. 2005;16(10):2346-53.
98. Alahmadi NS, Betts JW, Heinze T, Kelly SM, Koschella A, Wadhawan JD. Synthesis and antimicrobial effects of highly dispersed, cellulose-stabilized silver/cellulose nanocomposites. RSC Adv. 2018;8(7):3646-56.
99. Schulte M, Hensel M, Miskiewicz K. Exposure to stressors and antimicrobials induces cell-autonomous ultrastructural heterogeneity of an intracellular bacterial pathogen. Front Cell Infect Microbiol. 2022;12:963354.
100. Peterson E, Kaur P. Antibiotic Resistance Mechanisms in Bacteria: Relationships Between Resistance Determinants of Antibiotic Producers, Environmental Bacteria, and Clinical Pathogens. Front Microbiol. 2018;9:2928.
101. Chu EK, Kilic O, Cho H, Groisman A, Levchenko A. Self-induced mechanical stress can trigger biofilm formation in uropathogenic Escherichia coli. Nat Commun. 2018;9(1):4087.
102. Allocati N, Masulli M, Di Ilio C, De Laurenzi V. Die for the community: an overview of programmed cell death in bacteria. Cell Death Dis. 2015;6(1):e1609.

8. Appendix

8.1 Appendix 1

The following Figure presents the graphs of the bacterial growth of PAO1 (black curve) cultured at 42º C, at different optical densities [A (OD = 0.1); B (OD = 0.2); C (OD = 0.5); D (OD = 1.0); E (OD = 1.5); F (OD = 2.0)] and the corresponding supernatant at specific times where DCIP was added (black dots on violet curve).

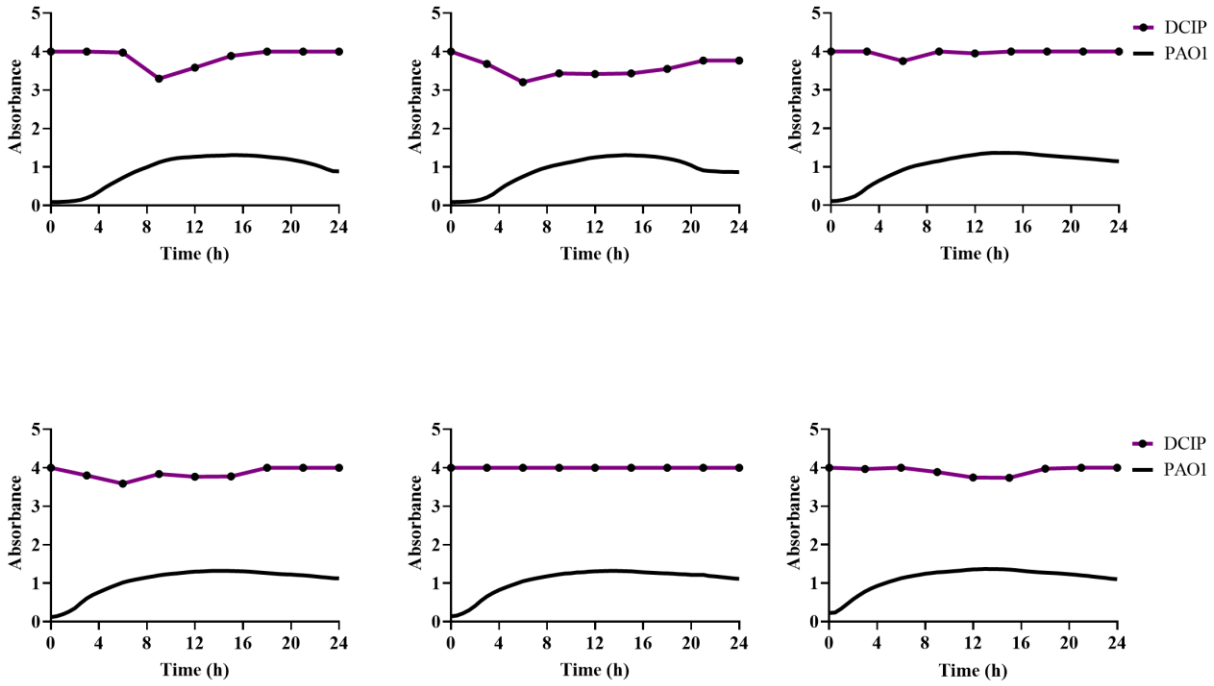

8.2 Appendix 2

The following Figure presents the growth curves of the Gram-negative bacterial strains tested (*E. coli* and *K. pneumoniae*) after 24 h treatment with GNP9.24.58, GNP8.24.50 and GNP9.24.50 at different concentrations.

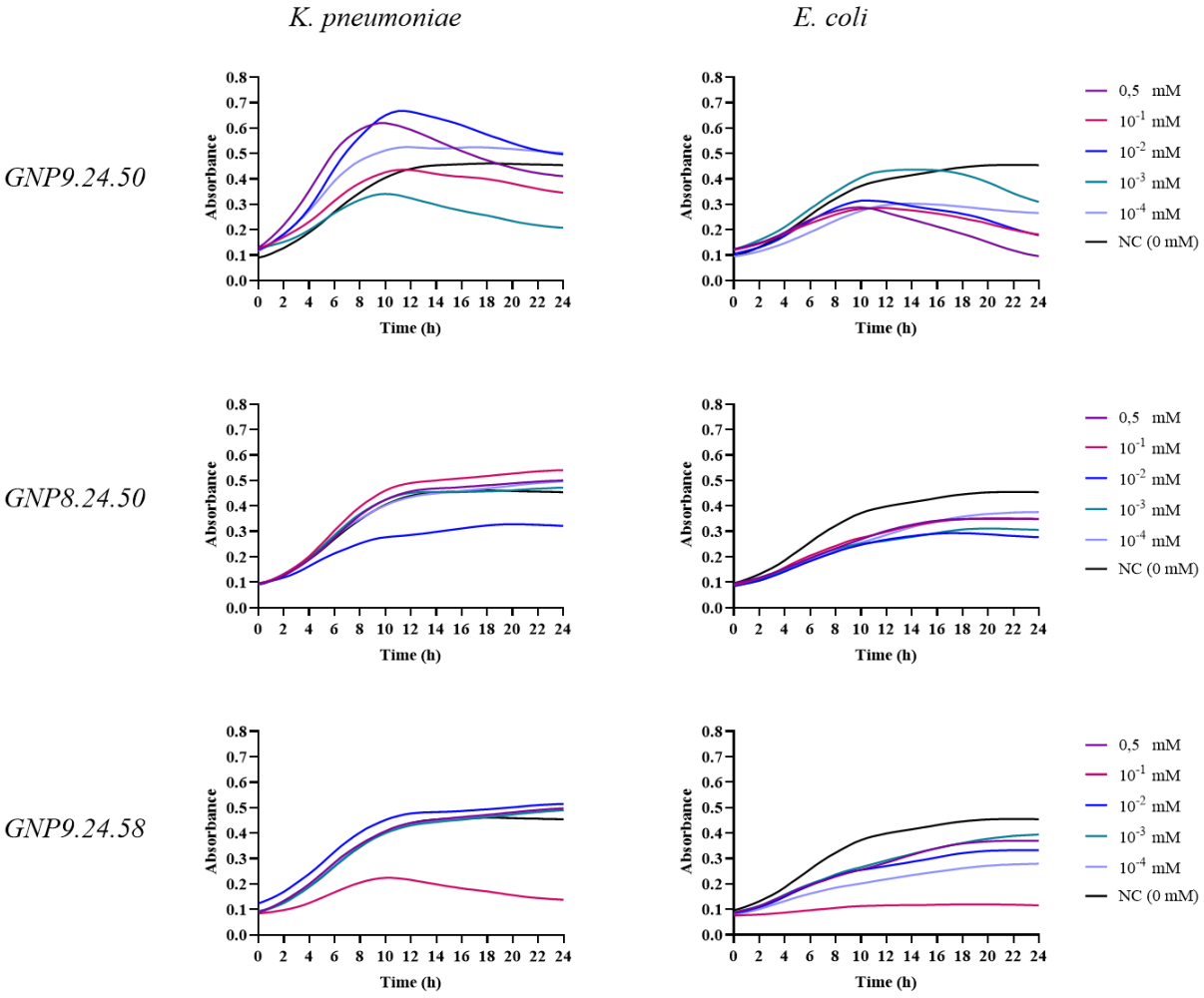

8.3 Appendix 3

The following Figure presents the growth curves of the Gram-positive bacterial strains tested (MSSA and MRSA) after 24 h treatment with GNP9.24.58, GNP8.24.50 and GNP9.24.50 at different concentrations.

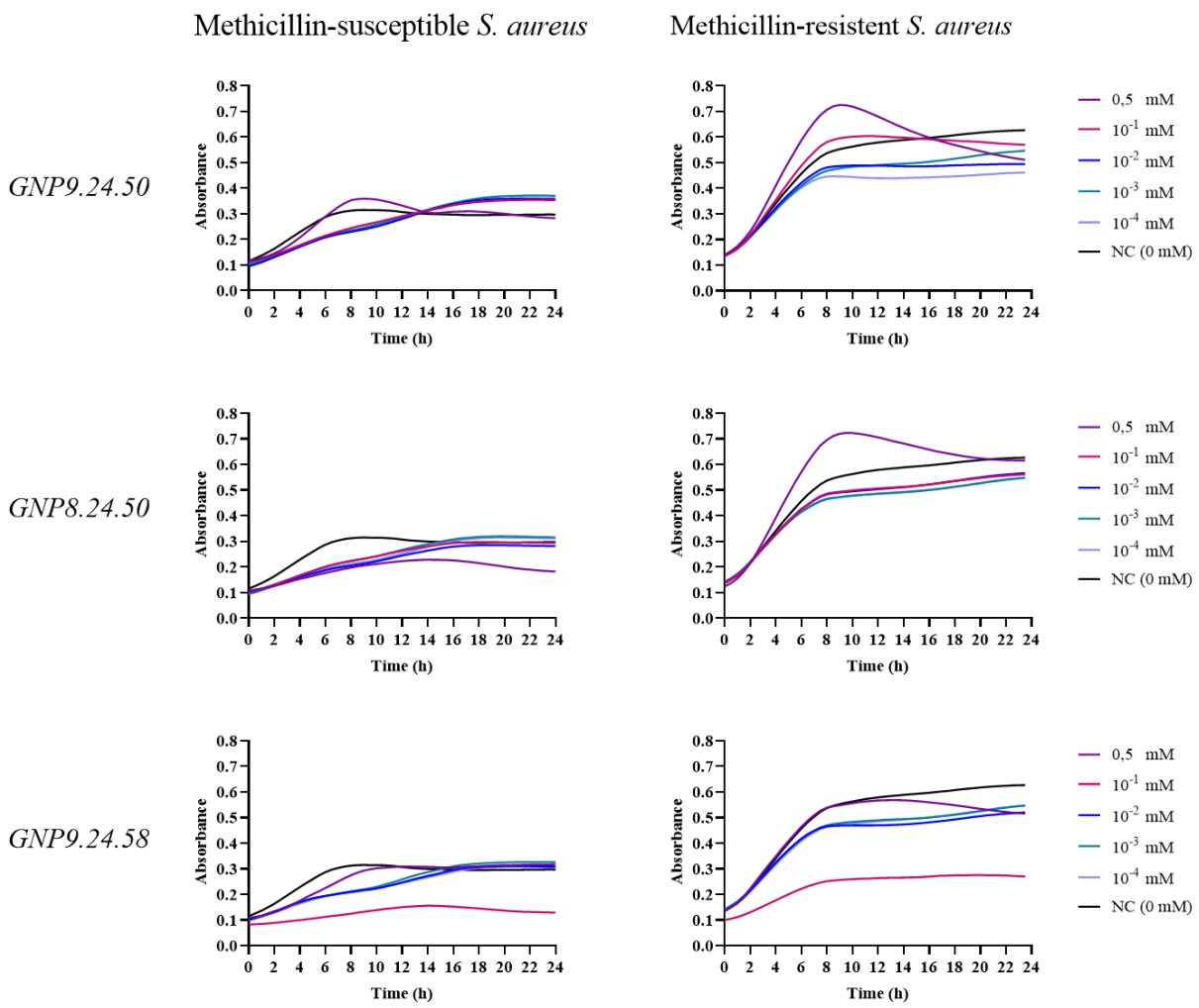

8.4 Appendix 4

The following Figure presents the relative total growth of the Gram-negative bacterial strains tested (*E. coli* and *K. pneumoniae*) after 24 h treatment with GNP9.24.58, GNP8.24.50 and GNP9.24.50 at different concentrations.

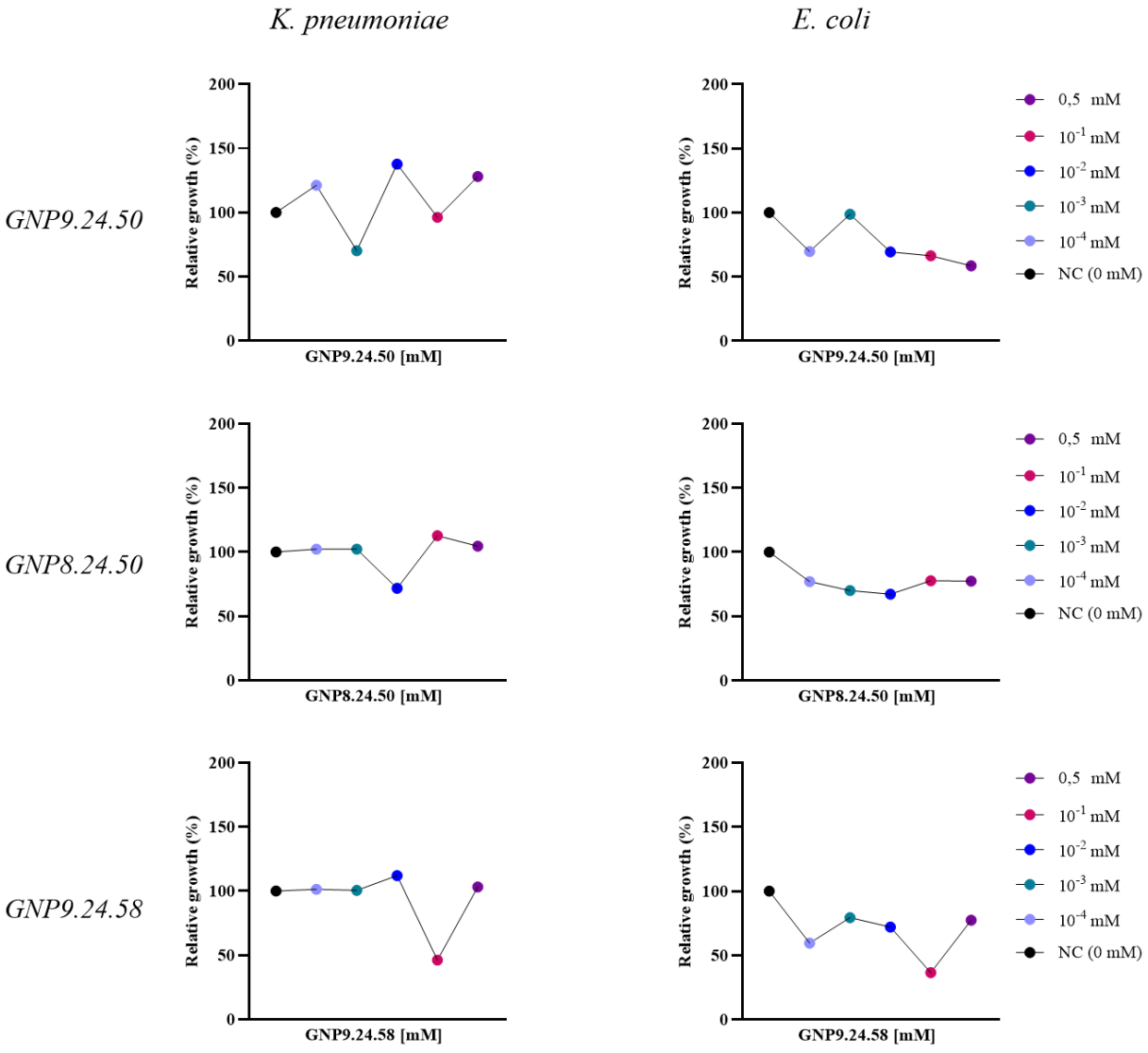

8.5 Appendix 5

The following Figure presents the relative total growth of the Gram-positive bacterial strains tested (MSSA and MRSA) after 24 h treatment with GNP9.24.58, GNP8.24.50 and GNP9.24.50 at different concentrations.